3D Electrode Array for Single-cell selectivity in Visual Prosthesis

Diego Lujan Villarreal (diego.lujan@tec.mx)
Instituto Tecnologico y de Estudios Superiores de Monterrey https://orcid.org/0000-0002-7917-039X
Wolfgang H. Krautschneider
Technische Universitat Hamburg

Research

Keywords: 3D electrode array, Retina Implant, Single-Cell Selectivity, 3D Retinal Reconstruction

Posted Date: April 1st, 2020

DOI: https://doi.org/10.21203/rs.3.rs-17767/v1

Title: 3D Electrode Array for Single-cell selectivity in Visual Prosthesis

Authors: Diego Lujan Villarreal, diego.lujan@tec.mx, Tecnológico de Monterrey, Escuela de Ingeniería y Ciencias. Av. Eugenio Garza Sada 2501 Sur, Tecnológico, 64849 Monterrey, Nuevo León, México. Wolfgang H. Krautschneider, krautschneider@tuhh.de. Hamburg University of Technology, TUHH, Hamburg, Germany
Corresponding autor: Diego Lujan Villarreal, diego.lujan@tec.mx

Abstract

Background: Visual prostheses electrically stimulate nearby neurons to generate artificial vision in patients blinded by retinal degenerative diseases. Current prosthetic devices offer limited spatial resolution that results in unselective stimulation of retinal ganglion cells (RGCs). This can be understood as a falling short of visual prosthesis to generate a complete visual scene with detail perception. In this report, the 3D linear electrode carrier is introduced. Our analysis develops a proof of principle to identify the usefulness of the 3D array to activate selectively single RGCs using small electrode size at the highest-density cell.

Methods: A simulation framework was built by locating the 3D linear electrode carrier with the highest-density cell. Stimulation of the 3D carrier is implemented at horizontal meridian in the superior retina within the region of 1 mm away from the fovea centralis. Stimulation in that space is needed for critical functions such as object recognition, reading, and driving. The simulation framework obeyed the RGC density and distribution, ganglionic layer thickness, vertical distribution and cell diameter at the fovea. To verify RGC electrical stimulation, the relevant retinal interface elements and dynamics of the voltage-gated ionic channels were integrated into a 3D computational model in COMSOL Multiphysics.

Results: the distribution of stimulus from a single active electrode to ground generates a volume of stimulation equivalent to the volume contained by a single RGC at the highest-density cell. Sensitive retinal tissue is safeguarded from electrochemical reactions caused by excessive charge density, the formation of corrosion and neural tissue heating since the advanced technology of the 3D array injects low thresholds for effective stimulation.

Conclusions: The 3D electrode array can provide a safe stimulus to enhance visual resolution that can be delivered by +1000 electrodes. This is required in humans for activities where visual detail is of primary importance and thus relevant for high-resolution vision. The 3D electrode array reveals small proximities of electrodes to cells for activation. This is of an advantage for cells located near and very-deep in the ganglion layer because low thresholds are injected to the electrodes producing a well-defined localization of stimulus, an independent activation that targets single RGCs and a safe stimulus.

Keywords: 3D electrode array; Retina Implant; Single-Cell Selectivity; 3D Retinal Reconstruction.

1. Background

Visual prostheses are designed to restore some vision to patients blinded by photoreceptor degenerative diseases, such as retinitis pigmentosa and age-related macular degeneration [Humayun et al., 1996]. The upgrade of visual prosthetic devices has been a followed subject since current status on clinical trials has not exhibited an array of independent phosphenes. Visual prosthesis would ideally generate an array of circular-shaped percepts with narrow dimensions that would represent a building block for the pattern of visual perception. Three of the major problems with current visual prostheses are the 1) use of large electrodes that misdirect the stimulus and create phosphenes with shapes other than a small spot of light, 2) incapability to adapt electrode stimulation at locations with high RGC density and 3) atypical patterns of retinal activity are induced by stimulation [Stingl et al., 2013; Humayun et al., 2018]. This presumably may be the cause that patients do not obtain a complete visual scene composed of simultaneously presented percepts using current retinal implant devices. Current prosthetic devices developed by [Mahadevappa et al., 2005; Reinhard et al., 2006; Rizzo III et al., 2003; Humayun et al., 2012; Stingl et al., 2013; Klauke et al., 2011] use large-sized electrode diameter of 500, 200 and 100 µm. The large diameter of stimulating electrodes in such implanted devices likely activates hundreds or thousands of cells over their area of stimulation. Not only this coarse stimulation of cells restricts the detail perception, but also the activity generated by stimulation remains dissimilar from a healthy retina. Electric current fields from relatively large electrodes indiscriminately drive local retinal circuits in an unnatural way, leading to complex retinal responses [Horsager et al., 2011].

Visual and spatial perception of retinal prosthesis demands small electrode usage to independently activate ganglion cells and replicate natural patterns of activity in the retina [Jepson, 2013; Fried et al., 2006]. Small-electrode size can allow the excitation of small groups of cells. However, the sensitive retinal tissue is exposed because of the required charge density activation by small electrode dimensions [Lujan et al. (b), 2017]. Safe

charge density limit is currently a major concern [Lujan (a), 2016; Lujan (b), 2016; Kasi et al., 2011; Horsager et al., 2011]. For detail recognition, the resolution of implants must be improved. This can be achieved by increasing both the number and density of electrodes [Weiland et al., 2014]. There is plenty of evidence that a high number of electrodes ranging from 625 [Cha et al., 1992] to 1000+ [Chader et al., 2009] can enhance visual resolution originated by electrical stimulation. This insight is well-correlated to upgrade mobility, independent living and walking in crowded environments [Cha et al., 1992], face recognition [Thompson et al., 2003], reading large-sized letters [Bagnoud et al., 2001; Dagnelie et al., 2006; Chai et al., 2007].

The proximity of cells to the electrodes plays a major role to activate nearby cells [Lujan et al. (b), 2017]. Close proximity reduces threshold current and charge density, producing a well-defined localization of stimulus. Despite that safe stimulus can be delivered from the electrodes by approaching them to the retina surface, however, surgical challenges are present to maintain the proximity as close as possible. Distant proximity contributes to the varying current spread from electrodes causing an increment in the volume of stimulation [Lujan et al. (b), 2017] and compromising visual resolution [Kasi et al., 2011]. The proximity between the implant and the retina also increases the possibility of thermal damage caused by the dissipated heat from the implant [Zrenner, 2002]. Large electrode diameter can safeguard sensitive retinal tissue against irreversible reactions at the electrode interface. This technique is frequently used in current visual devices [Mahadevappa et al., 2005; Eger et al., 2006; Rizzo III et al., 2003; Humayun et al., 2012; Klauke et al., 2011]. However, bundles of cells are activated by a single electrode leading a low visual resolution. Therefore, a trade-off is exhibited between reaching better quality of visual resolution and safety.

Electrode array topology influences the shape and breadth of the phosphenes while the retina is electrically stimulated [Lujan et al. (b), 2017]. That is, by applying a given value of peak stimulus amplitude, the current spread varies according to the topology of the electrode array and the position of the active and ground electrodes. This could lead to changes in the area of stimulation, thereby causing the generation of phosphenes with shapes other than a small spot of light. Thus, electrode topology is fundamental to restrict the stimulus to the space required for producing round dot-like percepts. Experiments performed with different electrode topologies revealed dissimilar shapes of phosphenes e.g. elongated shapes [Brindley et al., 1968; Rizzo III et al., 2003], triangles [Veraart et al., 1998], lines/bars [Rizzo III et al., 2003; Wilke et al., 2011], doughnut-shaped [Humayun et al., 2003], complicated patterns [Veraart et al., 1998] and round spots of light [Humayun et al., 2003; Mahadevappa et al., 2005; Rizzo III et al., 2003]. Table 1 lists the visual prostheses currently implanted in humans or isolated primate retinas with their quantity information of electrode number, diameter, and spacing.

Currently, visual prostheses transmit the stimulus from a flat 2D surface electrode array expecting to stimulate selectivity a single RGC [Jepson et al., 2013 & 2014]. Photomicrographs of the retina of healthy human [Kolb et al., 1995; Ross et al., 2003], monkey [Boycott et al., 1969] and mice [Ong et al., 2001] showed that the peak volumetric density of RGCs along the vertical section leans towards the middle of the ganglionic layer, leaving few RGCs neighboring the boundary with the vitreous medium. These findings suggest that considering the stimulation of nearby RGC to the electrode array as the sole assumption for high visual resolution may result in a clear misdirection and a misrepresentation of the natural spatiotemporal patterns of activity in RGCs of a different type. To achieve a near-normal vision, the diameter and density of stimulation electrodes must approach the size and density of the cells designed to stimulate [Sekirnjak et al., 2008]. Truthful restoration of natural RGC activity is likely to require independent activation of different cells. More specifically, a clear exhibition of independence would be selective stimulation of a single cell without activating simultaneously neighboring cells of any type [Jepson et al., 2013]. Previous work on the isolated retina [Jepson et al., 2013; Hottowy et al., 2012] indicated that single-cell selectivity is possible for some RGCs using electrode arrays with much higher density and smaller electrodes than clinical prostheses. Jepson showed in principle the possibility to activate safely single RGCs in the high-resolution visual pathways (highest-density cell) at their native spatial and temporal resolution. These results revealed direct stimulation of ON and OFF midget, ON and OFF parasol, and small bistratified RGCs using 15 μm electrode diameter and small current pulses that provide safe charge density range. [Fried et al., 2006] supported the use of small electrodes to activate small groups of cells, leading to rich resolution patterns of artificial-induced activity at the retina. Decreasing electrode dimensions generate higher resolution patterns of prosthetic-elicited activity that are closer to light elicited patterns. However, single-cell selectivity of RGCs will require higher-density electrode arrays, novel electrode geometries, and more sophisticated stimulation patterns [Grumet et al., 1999; Rattay et al., 2004].

TABLE 1 VISUAL PROSTHESES CURRENTLY IMPLANTED IN HUMANS OR ISOLATED PRIMATE RETINAS

Visual Prosthesis	Number of Electrodes	Elect. diameter [μm]	Electrode spacing[2] [μm]	Ratio of Electrode diameter to RGC Diameter[6]
Argus I [Humayun, 2001]	16	520, 260	800	52, 26
[Rizzo III, 2003]	20	100	620	10
[Rizzo III, 2003]	100	50	220	5
[Mahadevappa, 2005]	16	500	800	50
[Reinhard, 2006]	24	100	750	10
IMI [Hornig, 2007]	49	100, 360	75, 80[3]	10,36
Bionic Vision [Honert, 2007]	33	600	900	60
[Rodger, 2008]	60	75	[5]	7.5
EPI-Ret3[1] [Roessler, 2009]	25	100	500	10
Argus II [Humayun, 2012]	60	200	575	20
[Keseru, 2012]	12	50, 200, 360	[5]	5, 20, 36
[Jepson, 2013]	61	15	60	1.5
[Lohmann, 2019]	250	100, 1000[4]	520, 300[3]	10, 100

[1]Climical trials stopped, the company is presently closed. [2]Spacing is center-to-center. [3]Different spacing in electrodes. [4]100 and 1000 μm electrode diameter of active and ground electrodes, respectively. [5]Electrodes segmented into concentric circles. [6]RGC diameter of 10 μm is assumed.

As for the technology of advance electrode carriers, [Rodger et al., 2008] designed, fabricated and implanted in animals a biomimetic retinal parylene C-based electrode array with 60 of 1024 75 μm-diameter electrodes connected through dual-layer process. The biomimetic retinal array was able to stimulate tissue, elicit a response similar to the response generated from a light pulse and confirm excellent biostability. Although that the biomimetic retinal array retained the spherical curvature of the retina and produced a complex biomimetic pattern that closely mirrored the area density distribution of RGCs in the human retina [Curcio et al., 1990], the reasoning of how the biomimetic pattern is generated is incomplete. RGCs found in the human ganglion cell layer [Curcio et al., 1990] are not distributed along the border between the ganglion layer and the vitreous chamber but along the three-dimensional space of the ganglion layer that makes the volumetric density of cells. Peak volumetric density is not in contact with the border between the ganglion layer and the vitreous chamber but leans toward the boundary between the ganglion layer and the inner nuclear layer [Kolb et al., 1995; Ross et al., 2003; Boycott et al., 1969; Ong et al., 2001]. These findings suggest that considering the area cell density as the only assumption could result in a clear misdirection of electrode stimulus to empty regions of cells, a misuse of electrodes and a misrepresentation of the nature of cell distribution.

[Lohmann et al., 2019] designed the star-shaped very large electrode array for retinal stimulation or VLARS-design. The implantation surgery was established in cadaveric porcine eyes. To analyze biocompatibility, ten rabbits were implanted with the device. Any movement after implantation had to be done with great caution since the epiretinal VLARS was not fixated with a retinal tack. On the electrode array design, the proximity between active electrodes varies on their position, i.e. approximately 520 μm on the wings versus 300 μm in the center). The VLARS-design supports 250 individual electrodes, each having a diameter of 100 μm except to the solely larger return electrode located at the base of the connecting lead of the array with a diameter of 1mm [Waschkowski et al., 2014]. Although the VLARS results on a complete array diameter of 12 mm that covers approximately 110 mm^2, and a visual angle of 37.6° (corresponding to a visual field of 18.8°), the geometric mathematical reasoning of the electrode array design was misdirected to target single-cell selectivity. That is, the analogy between the volume covered by the current density distribution per electrode and the volume per RGC was neglected.

Argus I and II epi-retinal prostheses (Second Sight Medical Products, Inc, Sylmar, CA) implanted in patients reported streak-like visual percepts rather than a natural more commonly reported punctate-shaped phosphenes, suggesting a direct stimulation of axonal bundles [Humayun et al., 2012]. This is to be expected considering that the study used large electrodes of 200 μm of diameter and located far from the ganglionic layer (~180μm), necessitating over large amplitudes of current to reach RGC stimulation thresholds. As for experimental testimonies, both Argus II and Alpha IMS (Retina Implant AG in Germany) patients cannot perceive uncomplicated forms and letters instantly; rather they scan their head over objects to judge what they are seeing [Weiland, 2014]. In previous clinical trials of both sub- and epiretinal approaches demonstrate that patients do not experience such flawless pixelized sight as shown in many publications. An idea that each electrode produces a similar spot of light as compared with its neighbor is not completely the case. Argus II clinical trial demonstrated that 55% of single electrodes were capable to produce a spot of light within the safe boundaries

[Da Cruz et al., 2013]. It is clear, however, patients have at least some spatial information of the surrounding. Alpha IMS patients could read letters form a reduce set [Stingl et al., 2013]. Nevertheless, the control of the implant upon spots of light is not precisely consistent.

This paper introduces the 3D electrode array technology for retina implants (European Patent No. WO/2019/057551 [Lujan et al., 2018]). Our study develops a proof of principle strategy to pinpoint the usefulness of a 3D electrode array to activate selectively single RGCs utilizing small electrode size at the highest-density cell. This can be helpful for a truthful restoration of natural RGC activity [Sekirnjak et al., 2008; Fried et al., 2006; Jepson et al., 2013; Grumet et al., 1999; Rattay et al., 2004; Weiland et al., 2014]. Our simulation framework places the 3D electrode array 1 mm away from the fovea at the peak density of RGC. This is a requisite in visual prostheses because actions that require visual detail are processed within ±15° of eccentricity. We consider a three-dimensional reconstruction of the ganglion layer with realistic a) density distribution of RGCs along the retina, b) distribution of RGCs in the vertical section, c) diameter of RGC and d) ganglionic layer depth as a function of the eccentricity along the retina. Depth accuracy stimulation is examined at the peak volumetric density of RGCs along the vertical section at the ganglionic layer. To provide functional vision, we investigated safe stimulation of an existing ASIC design that can provide 1024 electrodes with low power consumption [Meza-Cuevas et al., 2014]. Electrochemical reactions of neural tissue heating from the retina implant, water-voltage window, and charge density injection limits were included in our study.

2. Materials and Methods

2.1 Linear Carrier Element

3D linear carrier element (LCE) as shown in Fig. 1(a) is connected to an electrode connecting point and carrying a plurality of the electrodes. The electrodes carried by a linear carrier element are arranged along a substantially straight line to penetrate into or through the surface of the ganglionic layer. Due to the close proximity to RGC, the electrodes can stimulate straightforwardly a single RGC with low injected current. In any event, the 3D linear carrier element can facilitate the desired placement of the electrodes within the respective retinal layer. For implantation, the dimensions and mechanical properties of the 3D linear carrier element may be selected such that its placement within the retinal tissue would not cause substantial damage to the nerve cells.

2.2 Electric Field Response and Nonlinear Response of Cell Neurons

A 3D computational model of electrical stimulation was implemented in COMSOL Multiphysics software (COMSOL, AB., Sweden, Version 4.4). The model consists of tissue boxes that represent a segment of the human eye, see Fig. 1(b). This schematic representation of the retina is built to a greater degree of anatomical likeness than previously published works [Kasi et al., 2011; Yin et al., 2010; Abramian et al., 2012; Werginz et al., 2015]. The layers included in the simulation model are the polyimide carrier of the electrodes, linear carrier elements, vitreous medium, photoreceptor layer, ganglionic layer, inner nuclear layer, ganglion cell soma, and retinal pigment epithelium. Electrical parameters and sizes of each layer are listed in table 2 [Kasi et al., 2011; Yin et al., 2010; Abramian et al., 2012; Werginz et al., 2015]. An arrangement of a single pair of electrodes consisting of an active and ground is implemented using epi-retinal design.

Single, monophasic linear decrease pulse shape of uniform current is injected from active to the ground electrode to drive cell activation. This externally applied current density is distributed to the retinal tissue and the participating channel types found in this particular RGC membrane. In this present study, we implemented in COMSOL Multiphysics the membrane model developed by [Fohlmeister et al., 1990]. The basic mathematical structure for voltage-gated ion channels was based on the equations developed by [Hodgkin & Huxley, 1952]. Four conductances associated with voltage-gated channels were considered: calcium gCa channel; sodium gNa channel; non-activating K+ (delayed rectifier) gK; inactivating K+ (A-type) gaK; calcium-activated K+ gkCa channel was gated by calcium Ca2+ and modeled on that basis. Recent works used this modeling assumption for the mathematical model of Hodgkin and Huxley [Joucla et al., 2014] and the model of RGCs [Lujan et al. (a), 2017]. The parameters and equations that describe the dynamics of the ionic channels were kept as in the original model [Fohlmeister et al., 1990]. We assumed that the peak boundary current density in the RGC membrane serves as an input parameter in the RGC circuit modeling. Hence, the peak boundary current density across the RGC membrane computed in Comsol Multiphysics is assumed to be equal to the extracellular current density of the circuit modeling. Threshold injected current required for RGC activation by means of extracellular stimulation must generate a voltage shift of around +30 mV in the RGC

membrane. Retinal network cells (i.e. bipolar, horizontal and amacrine cells, ON- and OFF networks) are excluded because the severe rod and cone photoreceptor impairment cannot drive visual phototransduction process started light photocurrent input.

2.3 Ganglionic Layer Thickness and RGC Diameter

[Raza et al., 2015] measured the ganglion layer thicknesses for 43 eyes of 36 human healthy controls. In this study, the data found by Raza was used in the reconstruction of the ganglion layer. In this present work, the distribution of RGC diameter found by [Ryskamp et al., 2011] and [Rossi et al., 2017] is used in the reconstruction of the ganglion layer.

2.4 Vertical Distribution of Retinal Ganglion Cells

Photomicrographs of the retina of healthy humans [Kolb et al., 1995; Ross et al., 2003], monkey [Boycott, 1969] and mice [Ong et al., 2001] were considered in the estimation of the RGC distribution along the vertical section. The ganglionic layer was divided in horizontal segments of equal thickness and cell nuclei were counted for each segment. Then, the results were averaged, normalized and plotted in red with circular markers against the thickness of the ganglionic layer, see Fig. 1(c). The normalized results of each reference are shown in black using four different line styles. The curve shape of the averaged and normalized data was fitted to a 3rd order polynomial and plotted in red with a solid line. The curve peak amplitude, not included in Fig. 1(c), was built such that the integral of the polynomial over the RGC thickness yields the same realistic amount of cells per mm^2 measured by [Curcio et al., 1990]. Thus, the polynomial

$$Az^3 + Bz^2 + Cz + D \qquad \text{(Eq. 1)}$$

describes the volumetric cell density with numerical values of D = 0, C = 3.7392 ρ_c/t^2, B = 0.741 ρ_c/t^3, A = -4.4802 ρ_c/t^4, where t is the RGC thickness. ρ_c is the area cell density. Here we assumed that the cell distribution along the vertical section behaves the same for all four meridians.

2.5 Investigation of Electrode Stimulation

The present work focuses on meridian maps of area cell density along the horizontal meridians (nasal and temporal) in the superior direction. This is mainly because 1) the highest ganglion cell densities are found in the horizontal meridian and 2) in peripheral retina densities in superior retina exceed those at the corresponding eccentricities in the inferior retina by 60% [Curcio et al., 1990]. Following the findings by Curcio, the peak cell density is found about 1 mm from the foveal center. At greater eccentricities within the central retina, ganglion cell density falls off with eccentricity more rapidly along the vertical meridian than along the horizontal meridian. Let us then obey the RGC density and distribution [Curcio et al., 1990], ganglionic layer thickness [44], vertical distribution [Kolb et al., 1995; Ross et al., 2003, Boycott, 1969, Ong et al., 2001] and the RGC diameter [Rossi et al., 2017; Ryskamp et al., 2011] at the location of 1 mm away the foveal center. Single localized excitation is examined by the stimulation of the 3D linear electrode carrier placed at horizontal meridians (nasal and temporal) in the superior direction. As such, 10µm ganglion cell diameter, 60µm ganglionic layer thickness and RGC area density of around 31,300 mm^{-2} are used in the reconstruction of the ganglion layer. Single electrode-cell stimulation is implemented with an electrode diameter of 7.5 µm. Electrode diameter around this dimension has been commonly used in ganglion cell stimulation [Dumitru et al., 2007; Chichilnisky et al., 2002; Jepson et al., 2014; Stett et al., 2007]. Here we assumed that the cell distribution along the vertical section behaves the same for all four meridians. The extent of the RGC stimulation is 4° (1 mm) where peak cell density is located. This boundary includes the region until 10° (2.7 mm) needed for critical functions such as object recognition, reading, and driving [Nelson et al., 2003].

2.6 Mathematical Approach for Single-cell Selectivity

Let us consider place the 3D linear electrode carrier at the location of 1 mm away from the foveal center, in the horizontal meridian (nasal and temporal) in the superior direction. This is equal to have a RGC density of 31,300 mm^{-2}, the ganglionic layer thickness of 60µm, RGC diameter of 10µm and a vertical distribution as seen in Fig. 1(c). RGCs located in the ganglion layer have their peak nearly in the center of their vertical distribution. Thus, the stimulating electrode array is placed about the middle of the ganglionic layer, see Fig. 1(b). The stimulating electrode array consists of one active and one ground electrodes. Single, monophasic linear decrease pulse shape

1(a)

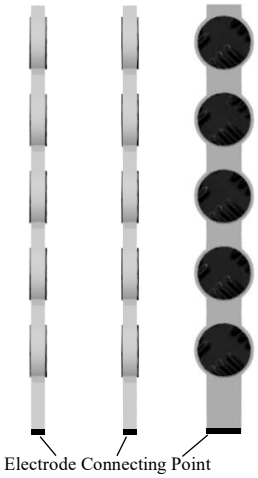

TABLE 2 DESCRIPTION OF THE VALUES OF SIMULATION

Layer	Conductivity [S/m]	Permittivity [-]	Thickness [µm]
Polyimide Carrier			10
LCE Length			60
LCE Depth	1e-17	1	2
LCE Outer Diameter[1]			9
LCE Width[2]			5
Vitreous Humor	1.5	98	50
Epithelium Layer	2e-3	1	65[1]
Photoreceptor Layer	28.5e-3	1	200
Intracellular space	10e-3	3.98e-11	30
PEDOT-NaPSS coating	400	1	0.2
Contact conductivity[3]	321	-	-
Cell membrane	1e-8	8.8e-11	0.01[4]
Inner nuclear layer	15e-3	1	100
Ganglionic Layer	10e-3	1	60

[1]Outer electrode diameter. [2]Width between electrodes. [3]Conductivity is of the contact of PEDOT-NaPSS deposition and tissue. [4]Cell membrane thickness.

1(b)

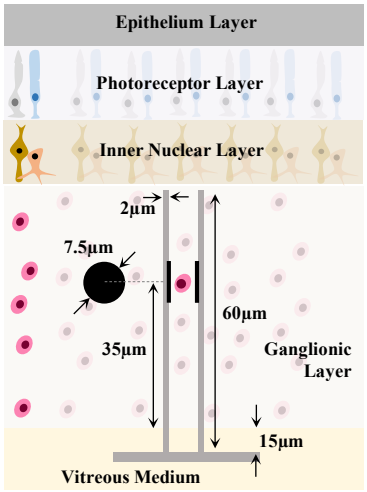

1(c)

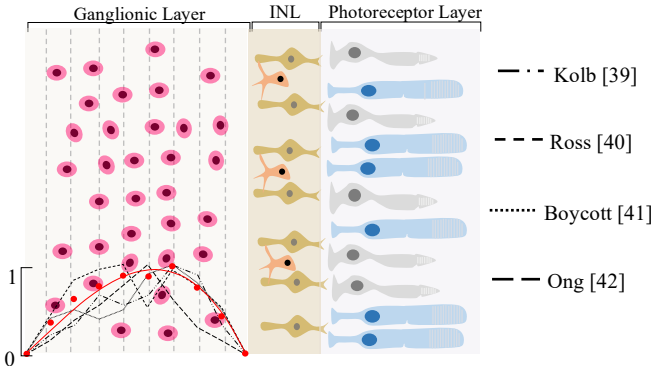

Figure 1(a) 3D linear electrode carrier connected to an electrode connecting point can carry a plurality of the electrodes. Electrodes are arranged along a substantially straight line to penetrate into or through the surface of the ganglionic layer. Fig. 1(b) 3D retinal model implemented in Comsol Multiphysics (not drawn to scale). The model consists of tissue boxes that represent a segment of the human eye. A single pair of electrodes involving an active and ground is implemented using epi-retinal design. Fig. 1(c) Sketch of the retina along the vertical section. INL is the inner nuclear layer. Cell nuclei counting results are shown as a function of the ganglion layer thickness. The averaged and normalized results are plotted in red with circular markers. The 3rd order polynomial is plotted in red with a solid line style. In addition, the normalized results of each reference are illustrated in black using four different line styles.

of 100µs is used. The mathematical approach for single-cell selectivity states that the current density distribution to the ground electrode generates the volume of stimulation that must be equal to the volume contained by a single RGC, and calculated as

$$v = \rho_v^{-1} \qquad \text{(Eq. 2)}$$

ρ_v is the volumetric cell density in µm^{-3}. The volumetric cell density at the vertical distribution can be computed as explained in (Eq. 1). The result of (Eq. 2) is called the stimulation cube. It is defined as a tridimensional space on the retina where the distribution of the stimulus initiated at the active electrode in effect triggers a response of a single cell. The criterion of the stimulation states that if stimulation of an electrode is achieved inside its volume, the cell is activated. Otherwise, the cell is not activated. Let us adopt that the cell distribution per volume is uniform in a manner that the volume can be represented as a cube with equal lengths calculated as the cube root of the cube volume

$$l_c = \sqrt[3]{v} \qquad \text{(Eq. 3)}$$

The proximity of neighboring face-to-face electrodes is equal to l_c.

2.7 Threshold of RGC Stimulation

The procedure for obtaining the threshold current density of a single RGC and the stimulation threshold for the cube is explained as follows. Single excitation of a RGC follows the placement of a cell inside the ganglionic layer, exactly between the linear carrier elements where the electrodes are located, see Fig. 1(b). This is arranged such that there is an equivalent distance from the RGC and the active and ground electrodes. Single RGC stimulation was investigated by increasing the peak stimulation current with an interval of 0.1 nano amperes until the action potential is generated. The stimulation threshold for the cube is as follows. A single cell is placed in several points of the cube, see Fig. 2(a), and peak stimulation current was increased with an interval of 0.1 nano amperes until the action potential is generated. Threshold values for each case are stored. To ensure an effective threshold value, this procedure was repeated six times to include all possible point alternatives. Afterward, the stimulation threshold for the cube was determined as the average of all threshold values. For both procedures are used a single pair of stimulating electrodes consisting of one active electrode and one ground.

2.8 Average Power Density and Neural Tissue Heating

The main objective of retinal stimulation, using either epi- or subretinal technique, is to provide a functional vision that comes from at least 1024 image pixels with at least 20 images per second. To achieve this request, the viability of using at least 1024 electrodes is studied by attaching 16 scalable chips of 64 electrodes each with a daisy chain configuration with low power consumption per Local Stimulation Unit (LSU) [Meza-Cuevas et al., 2014]. Biocompatibility was ensured for invasive electrodes by PEDOT-NaPSS coating [Starbird, R. et al., 2012]. The main target is within a time duration of $1/f$ to individually trigger at least 1024 pixels with pulse duration Δt and have a full image. For multiple stimulation, the control of selecting the role of electrodes to function as active or ground is considered as seen in previous publications [Meza-Cuevas et al., 2014; Lujan et al. (a), 2016]. Active electrodes can have their timeslot for stimulation.

The average power density of the device, P, is calculated considering the power of the transistors P_t that drive the electrodes used during the pulse of stimulation and the power per LSU, P_{LSU} [Lujan et al. (a), 2016]. P_t is calculated using a simplified electrical circuit of a retinal implantable device powered by a voltage source V_{DD}, (see Fig. 7 in [Lujan et al. (a), 2016]. P_t is given by:

$$P_t = \frac{e_{ON}}{2} I_a (V_{DD} - V_e) \qquad \text{(Eq. 4)}$$

I_a is the applied current. For sake of simplicity, we assumed that the voltage drop in the tissues is equal to the voltage drop across the electrodes, V_e. Each branch has two transistors that drive the active and ground electrodes, and the load associated with the tissue. Since each active or ground electrode is equivalent to one transistor [Meza-Cuevas et al., 2014], the total number of transistors is equal to $e_{ON} = 2(e_t \Delta t f)$. Since each branch contains two such transistors, the total number of branches is $e_{ON}/2$. These branches are activated per pulse duration Δt. e_t are the total number of electrodes. f is the total image frequency. We assume that the voltage drop in the branches is approximately the same and there is an equal distribution of current across the branches. The average power density at the device with units of [mW/cm^2] then is computed as follows

$$P = \frac{e_t \Delta t}{A_D T} (P_t + e_{ON} P_{LSU}) \qquad \text{(Eq. 5)}$$

$\Delta t/T$ defines the duty cycle of stimulation. T is the inverse of the total image frequency. A_D is the total chip surface area and P_{LSU} is the power consumption per electrode or LSU of 54μW [Meza-Cuevas et al., 2014]. The neural tissue heating from the retina implant is calculated using the average power density at the device in the linear approach of ΔT = 1°C per 12.2mW/cm^2 [Sohee et al., 2006] assuming only heat conduction. The initial temperature was a body temperature of 37° degrees.

Attaching 16 scalable chips of 64 electrodes each with a daisy chain configuration [Meza-Cuevas et al., 2014] can generate an implant device of at least 1024 electrodes. That is, each ASIC is equal to control of 64 electrodes. The dimensions of one ASIC consists of a width of 1.92mm and a length of 2.2mm. An additional 1 mm on each edge is added for wire bonding. Then, the total width, w, and the length, l, of a single ASIC is 3.94 and 4.2mm, all respectively. The total chip surface area is computed as wln_{ASIC}. Where n_{ASIC} represents the number of ASICs required in each case. For 1024 electrodes, a total chip surface area obtains 0.68 cm^2.

2.9 Stimulation Safety

Safety in terms of electrical performance is mainly related to three factors: charge density injection level, neural tissue heating due to the power dissipation by the device, and the water-voltage window. Electrolysis of water may occur as well as a result when the maximum cathodic and anodic potential across the electrodes surpass the "water window" boundary [Merrill et al., 2005]. The water window is a potential range that is defined by the reduction of water, forming hydrogen gas, in the negative direction, and the oxidation of water, forming oxygen, in a positive direction which may cause corrosion. High charge density is required by small electrode usage that can cause a breakdown of the electrode, adverse tissue reactions and gas bubbling evolution, which damage the soft retinal tissue layers [Brummer et al., 1977]. The neural interface devices must be shown not to cause significant temperature increases in the implanted tissue. As regards to visual prosthesis, the liquid environment of the vitreous humor acts as a heat sink that is capable of dissipating a significant amount of power. An electronic chip positioned away from the retina can run at considerably higher powers than a chip positioned on the retinal surface [Piyathaisere et al., 2003]. It is reported that maximum permissible temperature increase in the cortex is about 1°C or maximum power density is 80 mW/cm^2 of exposed tissue area [Seese et al., 1998]. [Rose & Robblee, 1990] applied platinum electrodes and brief pulses while measured a conservative charge density limit of 0.1–0.15 mC/cm^2 (cathodal-first biphasic) or 0.05–0.1 mC/cm^2 (anodal-first biphasic). Charge density limit of 0.1 mC/cm^2 is comparatively conservative. [Brummer & Turner, 1977] suggested that charge densities of up to 0.30–0.35 mC/cm^2 are safe for longer pulses to generate adverse electrochemical reactions at the surface of platinum electrodes. [Ray et al., 2011] in a recent study of high-frequency stimulation in rat retina found no significant histological changes to the retina up to 0.68mC/cm^2 with platinum electrodes. Argus II and Alpha IMS used platinum gray and titanium nitride respectively. Typical electrode material in neurostimulation is bulk platinum. The charge injection capacity for such material is 0.1-0.35 mC/cm^2. Platinum gray can inject up to 1mC/cm^2, and titanium nitride until 0.9mC/cm^2, which represents an important step for implantable bioelectronics. [Humayun et al., 2018]. Alternatively of platinum electrode material, iridium oxide may be used to prolong the range of charge densities that can be injected without inducing unwanted electrochemical reactions at the electrode surface [Beebe & Rose, 1988; Weiland et al.,2002].

In this study, electrochemical safety is examined in terms of charge density injection level, electrode voltage (or water-voltage window) and neural tissue heating due to the power dissipation by the device. Voltage window limit of 1.5 V assuming a PEDOT-NaPSS coat for invasive electrodes [Boretius et al., 2010]. Neural tissue-heating limit is 1°C based on circular electrode areas fell within the limits previously stated. Because the pulse shape used in this study was a monophasic linear decrease, we compared our activation thresholds to the midpoint of these safe charge density values of 0.1 mC/cm^2 for gas-free and erosion-free operation. For computing the average power density and the neural tissue heating, we extracted from Comsol Multiphysics the average peak stimulus density from the electrode and voltage across the electrodes. The charge density injected to the electrodes is calculated as

$$Q = \frac{1}{\pi r^2} \int_{t_0}^{t_f} I dt \qquad \text{(Eq. 6)}$$

r is the radius of the electrode, I is the peak threshold current injected along an initial and final time of stimulation t_0 and t_f, respectively. A Matlab script organized the extracted data and performed several tasks to obtain the heat dissipated by the device and charge density on the electrode. Peak threshold current density applied at the electrode is calculated by dividing the peak threshold current applied at electrode over the cross-section area of the electrode. Electrode potential is calculated internally in COMSOL Multiphysics.

3. Results

3.1 RGC Activation

The simplest stimulus is a single, monophasic linear decrease pulse shape. On top-left a zoomed-in view specifies the waveform until the final time of 100 μs, see Fig. 2(b). Action potential is triggered with a threshold peak stimulus of 0.5 nA that results in an average peak stimulus density of 11.31 A/m^2 from the electrode. Single RGC located between the active and ground electrodes obtains an average boundary-peak stimulus density of 3.1 A/m^2 for effective stimulation.

For the stimulation cube, a single RGC was located in six different points of the cube, see Fig. 2(a) and peak stimulation current is increased until membrane activation. The action potential is generated with an average threshold peak stimulus of 1.63 nA that results in an average peak stimulus density of 36.9 A/m^2 from the electrode, see Fig. 2(c) and Table 3. Effective membrane activation required different values of electrode peak stimulus as the RGC shifted its position along with the cube. Points (1), (2), (4) and (5) required peak amplitudes ranging between 43 to 45.3 A/m^2 applied to the RGC. Points (3) and (6) required small stimulus amplitudes varying between 22 to 23 A/m^2. This twofold increase of the electrode peak stimulus is mainly because of the close proximity of the RGC to the electrode. Single RGC located at six different points of the cube obtains an average boundary-peak stimulus density of 3.7 A/m^2 for effective stimulation using an interval of 0.1 nano amperes of peak electrode stimulus see Fig. 2(d).

3.2 Stimulation Safety

Natural RGC visual perception is attained by activating small areas of the retina [Jepson, 2013]. As a result, small electrodes are the topmost requirement because small groups of cells can be activated. Despite visual reception is improved; however, the exposure of sensitive retinal tissue must be safeguarded because of the charge density required by small electrode dimensions. The formation of corrosion [Fried et al., 2006], electrolysis of water [Merrill et al., 2005; Brummer et al., 1997] and significant damage to various cellular functions due to an excessive tissue heating [Sohee et al., 2006] must be avoided. Biocompatible materials with low impedance are essential because power consumption from an implanted retina device contributes to thermal rise while targeting cells are stimulated [Lujan, 2017].

RGC stimulation by the 3D electrode array can inject safe stimulus below the limits of electrochemical reactions to produce the stimulation cube (see Table 3). Average power density was calculated using a monophasic linear decrease pulse duration of 100 μs, a total number of electrodes of 1024, a total chip surface area of 0.68 cm2 and a total image frequency of 20 Hz. Power consumed by individual ASIC is 0.054 mW [Meza-Cuevas et al., 2014]. To drive that number of electrodes with that image frequency, it is required to activate simultaneously two active electrodes and two grounds for an individual pulse duration of 100 μs. Linear decrease waveform was selected by mainly two main reasons. According to [Meza-Cuevas et al., 2012], linear decrease indicated lower charge injection, dissipated energy and the corresponding voltage at the electrodes than the rectangular waveform required for stimulation. Secondly, the time-consuming in simulation in Comsol showed a maximum time of about 1.5 min.

RGC proximity to the electrode using the 3D electrode array is beneficial to minimize electrode peak stimulus for effective stimulation. This is advantageous to avoid irreversible reactions such as gas-bubbling formation caused by high injected charge densities, neural tissue heating produced by high power dissipation by the device, and the water-voltage window triggered by high electrode voltage. Small proximity of electrodes to RGC, as a result, allows electrodes to activate more likely a single cell. RGCs of different types can be independently stimulated without simultaneous activation of neighboring cells of any type. Accordingly, a truthful restoration of natural RGC activity that likely requires independent activation of different cells [Jepson, 2013] may be achievable using the 3D electrode array.

To date, electrode array requires major improvement for safe stimuli and visual acuity. Safe activation of RGCs requires high charge density threshold coming from small electrodes. Reason is that injected charge densities would increase the likelihood to produce gas-bubbling formation while electrode diameter is reduced. Small electrode dimensions can produce greater resolution patterns of artificial-elicited activity that are closer to light-elicited patterns [Cai et al., 2011]. RGC activation by the 3D array can reduce the threshold peak stimulus to the electrode and as a result, can reduce electrode size. Small electrode diameter can be applied, allowing selective excitation of small groups of ganglion cells.

Pulses shorter than 150 μs of duration which can replicate light-elicited spiking patterns; trigger solely a single spike with precise temporal pattern and send a more physiological signal to the brain [Fried et al., 2006]. [Jensen & Rizzo III, 2005] addressed this issue. In short, short-current pulses of 100μs or less showed significant preference because passing retinal ganglion cell axons can be avoided while stimulation. Choosing that pulse duration, the amount of current needed to generate the response of a cell is much lower than that required to generate an axonal response. [Greenberg et al., 1999] supported these observations by reporting that axonal

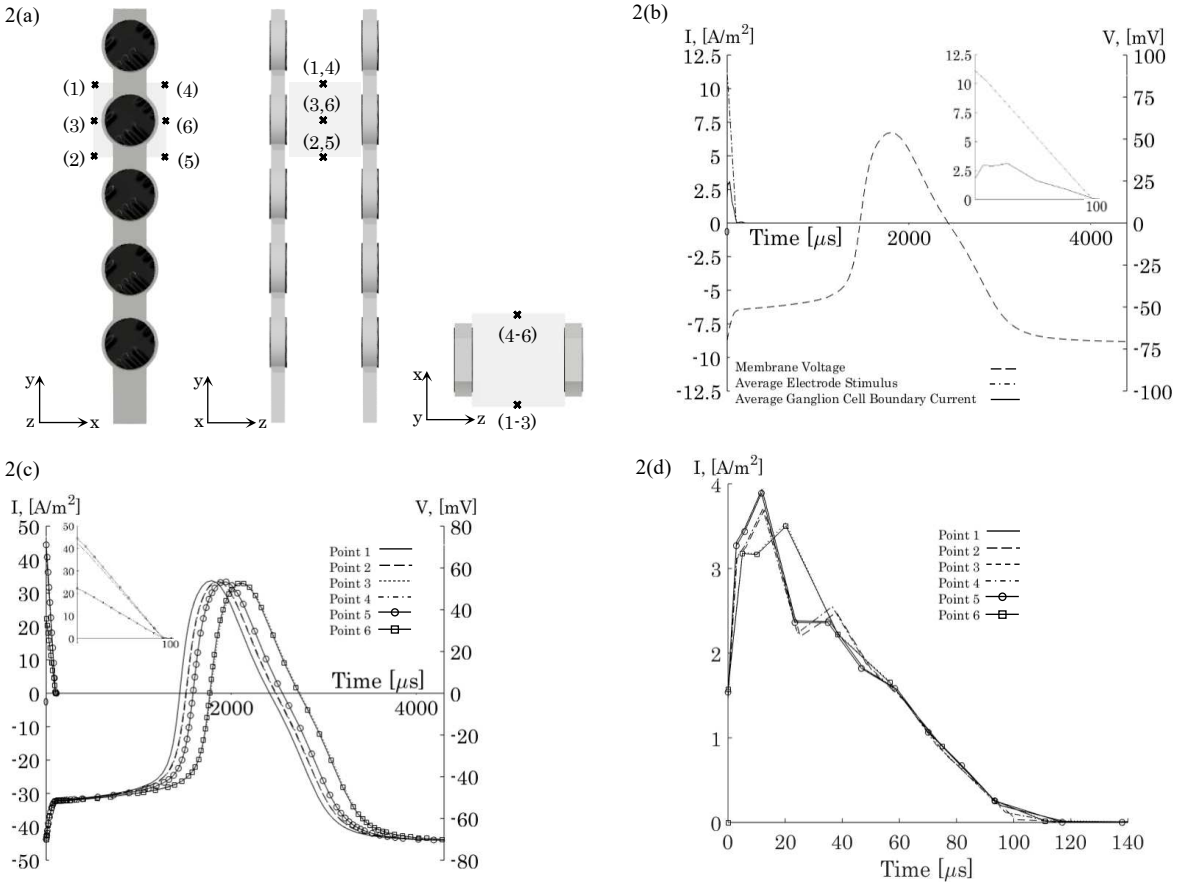

Figure 2(a) Six different points of the cube to investigate the threshold current from the electrode. Note that all points are repeated based on the coordinate of interest. Fig. 2(b) threshold current density for exiting a single RGC. The cell is placed inside the ganglionic layer exactly between the linear carrier elements where the electrodes are located. Action potential is triggered with an average peak stimulus density of 11.31 A/m^2 from the electrode. Single RGC located between active and ground electrodes obtains an average boundary-peak stimulus density of 3.1 A/m^2 for stimulation. Fig. 2(c) threshold current density for generating the stimulation cube. Single RGC was placed in six different points to investigate membrane activation. Action potential is generated with an average peak stimulus density of 36.9 A/m^2 from the electrode. Effective membrane stimulation required different values of electrode peak stimulus as the RGC shifted its position along the cube. Fig. 2(d) average boundary-peak stimulus density for effective stimulation of a single RGC located at six different points of the cube.

threshold was 20% higher than that of the retinal ganglion cell. Experimental findings by [Jepson et al., 2014] exhibited single spike responses with sub-millisecond latency, which is a characteristic of direct ganglion cell activation. In this study, short pulse durations of 100 μs and small electrodes of 7.5 μm of diameter were used.

3.3 Stimulation Cube Volume for Single-cell Selectivity

Volumetric cell density along the vertical section of the ganglionic layer is described by the solution of the third-order polynomial, see (Eq. 1). Current density distribution to the ground electrode specifies the generation of the stimulation cube volume, which is equivalent to the volume contained by a single RGC. The criterion of the stimulation states that if stimulation of an electrode is achieved inside its volume, the cell is activated. Otherwise, the cell is not activated. Stimulation cube volume computed as the reciprocal of the volumetric cell density applies a uniform cell distribution. This simplifies the representation of the cube with equal lengths computed as the cube root of the cube volume see Fig. 2(a).

Vertical volumetric RGC density in μm^{-3} is calculated as a function of the ganglionic thickness at the location of 1 mm away from the foveal center, in the horizontal meridian (nasal and temporal) at the superior direction. Through these results, the stimulation cube volume and length corresponding to the cube volume contained by a single RGC are computed. As previously stated, active and ground electrodes are located face-to-face in

TABLE # 3 RESULTS OF SIMULATION OF THE 3D ELECTRODE ARRAY

Data from Simulation / Point in Cube	1	2	3	4	5	6
Peak Threshold Current applied at Electrode (nA)	2	1.9	1	1.9	2	1
Peak Threshold Current Density applied at Electrode (A/m²)	45.27	43.01	22.64	43.01	45.27	22.64
Peak Threshold Boundary current density at RGC (A/m²)	3.9368	3.69	3.5386	3.7054	3.8889	3.5007
Electrode potential (V)	6.671E-03	6.349E-03	3.120E-03	6.498E-03	6.801E-03	3.110E-03
Power (mW/cm²)	6.703E-04	6.703E-04	6.703E-04	6.703E-04	6.70E-04	6.703E-04
Heating (°C)	5.494E-05	5.494E-05	5.494E-05	5.494E-05	5.49E-05	5.494E-05
Charge density (mC/cm²)	2.264E-04	2.150E-04	1.132E-04	2.150E-04	2.264E-04	1.132E-04

different linear carrier elements around the middle of the ganglionic layer. Reason is that peak volumetric density is located close to the center of the ganglion layer. Peak volumetric cell density obtains 8.05e5 mm^{-3} or 8.05e-4 μm^{-3}. Cube volume dimensions at the peak of the volumetric density obtain 1.24e3 μm^3 and an equal cube length of 10.75 µm. RGC diameter of 10µm is applied in the reconstruction of the ganglion layer. Stimulation cube volume and RGC sphere volume ratio of 2.4 represents the viability to locate the 3D electrode array without damaging the cells.

Current density penetration depth described by the time-dependent electrical current simulation of electrical current distribution in conductive and capacitive media was applied in our study. Stimulus from the electrode required an average peak-current value in the region of 36.9 A/m^2 to produce the stimulation cube for effective stimulation, see Fig. 2(c). Since 3.1 A/m^2 is sufficient to generate an action potential, the volume enclosed by that threshold average boundary-peak stimulus was directly obtained from (COMSOL Multiphysics, Version 5.3) using the surface/contour feature (see Fig. 3). The white line in the plots represents the zone of current penetration depth for stimulation across the geometry. Dashed-line squares represent accurately the dimensions of the stimulation cube. Groups of planes (*zx*, *xy*, *yz*) illustrate the electrical current distribution in conductive and capacitive media at a time of 10 µs. Collectively, each group corresponds to seven sub-planes located at a distance of ($\pm l_c/2$, ±4e-6, ±2e-6) µm away from the center sub-plane. As a reminder, l_c represents the lengths of the cube calculated as the cube root of the cube volume $\sqrt[3]{v}$. Stimulation cube is assembled by equal lengths l_c of a value of 10.75 µm assuming a volumetric cell density of 8.05e5 mm^{-3}.

4. Discussion

In this study, the 3D electrode carrier is introduced. RGC localized stimulation is examined as the 3D carrier is placed at horizontal meridians (nasal and temporal) at the superior direction with the highest volume density of RGCs. In brief, our results indicate that electrode stimulus utilizing the 3D carrier generates a volume of stimulation equivalent to the volume contained by a single RGC. Excitation of a small volume of the retina allows a more natural visual perception and replicates truthful spatiotemporal patterns of activity in the retina. The exposure of sensitive retinal tissue caused by electrochemical reactions is safeguarded as a result of injecting low thresholds for effective stimulation.

4.1 Precise stimulation of very-near and deep ganglion cells

Ganglion cell types can be differentiated from one another based on morphological and physiological criteria [Cook, 1997; Rowe el al. 1977; Dacey, 1999]. Studies in the cat retina suggest there may be as many as 20 such RGC types [Enroth-Cugell et al., 1966; Boycott et al., 1974]. In a healthy retina, the brain collects different features of the visual scene by temporal patterns of activity in around 20 different RGC types that are spatially intermixed [Dacey et al., 2004]. Dacey reported four numerically dominant RGC types in the primate retina: ON parasol, OFF parasol, ON midget, and OFF midget, which cooperatively represents around 70% of the visual signal transmitted to the brain in primates. As a result, RGCs that are near one another often transmit very different signals. [Jepson et al., 2013] reported that the five numerically dominant retinal ganglion cell types (i.e. ON and OFF midget, ON and OFF parasol, and small bistratified ganglion cells) have similar activation thresholds. Besides, single cells could be precisely activated without stimulating adjacent RGCs of the same type or other types. Previous work on the isolated retina using electrode arrays with much higher density and smaller electrodes than clinical prostheses indicates that single-cell selectivity is possible for some RGCs. However, some RGCs could not be selectively activated, even in regions of the retina with relatively low ganglion cell density [Hottowy et al.,2012; Jepson et al.,2013]. Thus, although increases in electrode density and decreases in electrode size may enhance the selectivity of clinical devices, additional methods will likely be required to approach single-cell selectivity, particularly in the central retina where RGC density is high.

Computer simulations of RGC activation (see Fig. 3) illustrate the volume enclosed by the threshold average boundary-peak stimulus of 3.1 A/m^2 that was straightforwardly attained from COMSOL Multiphysics using the surface/contour feature. The white line in the plots represents the zone for penetration depth for stimulation across the geometry. Stimulus from the electrode required an average peak current value in the region of 36.9 A/m^2 to produce the stimulation cube. This is equivalent to deliver an average threshold peak stimulus of 1.63 nA from the electrode. This reflects the fact that the 3D carrier can accommodate individual electrodes very close to the cells for precise selective activation. Stimulation cube is assembled by equal lengths l_c of a value of 10.75 µm assuming a volumetric cell density of 8.05e5 mm^{-3}. As illustrated, groups of planes (*zx*, *xy*, *yz*) show dimensions comparable to the stimulation cube. This indicates that the 3D linear carrier could theoretically present an approach to enhance selective activation of targeting cells using visual prostheses.

Healthy human [Kolb et al., 1995; Ross et al., 2003], monkey [Boycott, 1969] and mice [Ong et al., 2001] photomicrographs of the retina indicates that RGC peak volumetric density leans towards the middle of the vertical section of the ganglionic layer, leaving few RGCs neighboring the surface of the electrodes, see Fig. 1(c). Typical 2D surface electrode array delivers radially the current density in the retinal tissues expecting to stimulate selectivity a single RGC. If achievable, accurate selective activation would stimulate RGC close to the carrier, see Fig. 4(a). However, cells located deeply in the vertical segment of the ganglionic layer would leave inactive. As a result, visual prostheses may induce responses that constitute of irregular patterns far from being natural patterns of prosthetic-elicited activity of the retina. This suggests that considering the stimulation of nearby RGC to the electrode array as the sole assumption for high visual resolution may result in a clear misrepresentation of the natural spatiotemporal patterns of activity in RGCs of a different type. Reason is that RGC types can be differentiated from one another based on morphological and physiological criteria [Cook et al., 1997; Rowe el al. 1977; Dacey et al., 1999]. Studies in the cat retina suggest there may be as many as 20 such RGC types [Enroth-Cugell et al., 1966; Boycott et al., 1974]. In a healthy retina, the brain collects different features of the visual scene by temporal patterns of activity in around 20 different RGC types that are spatially intermixed [Dacey et al., 1999]. Accordingly, RGCs that are near one another often transmit very different spatiotemporal signals. A suggestion to stimulate selectively RGCs by a flat 2D surface carrier may disregard significant contributions of bundles of cells and may reproduce inaccurately natural spatiotemporal patterns of activity of the retina. That is, accurate selective activation of RGC by 2D surface electrodes clearly provides complete negligence of cells placed deeply in the vertical segment of the ganglionic layer. This presumably may be the cause that patients do not obtain a complete visual scene composed of simultaneously presented percepts using current visual prosthetic devices.

As opposed to the 2D carrier, precise stimulation of very-near and deep RGCs can be realized with the advanced technology of the 3D electrode carrier, see Fig. 4(b). Reason is that 3D carrier technology can distribute the stimulus in a small volume equivalent to the volume contained by a single cell, generating the stimulation cube (for more information see Mathematical Approach for Single-cell Selectivity). Any cell positioned randomly in the vertical segment of the ganglionic layer can accurately be activated by low threshold stimulus, preventing the generation of electrochemical reactions. Natural RGC visual perception can be realized by activating small areas of the retina [Jepson, 2013]. As a result, small electrodes are the topmost requirement because small groups of cells can be activated. As an advantage, the 3D electrode array can minimize the peak threshold stimulus that allows the reduction of the electrode size to a degree that produces safe stimulation.

4.2 Electrode Carrier Dimensions and Total Chip Surface Area

The electrode carrier width can be calculated by applying the length of the stimulation cube as $l_c(e_i - 1) + e_d e_i$, where e_i is the number of rows of linear carrier elements and e_d represents the depth of the individual linear carrier. The electrode carrier length is computed as $l_c e_j$, where e_j is the number of columns of linear carrier elements. For a 16x16 array of linear carrier elements that collectively accommodate 1024 electrodes (four electrodes per linear carrier), the total electrode carrier width and length is 193 x 172 µm respectively, assuming a linear carrier element thickness of 2 µm. Since the cube volume dimensions at the peak of the volumetric density obtain 1240 µm^3 and an equal cube length of 10.75 µm, the individual linear carrier can accommodate as far as five electrodes in a 60 µm vertical thickness in the ganglionic layer. This would be equal to house 1280 electrodes. Our simulations suggested that that amount of electrodes can deliver safe stimulus by injecting low thresholds and generating volume of stimulation equivalent to the volume contained by a single RGC.

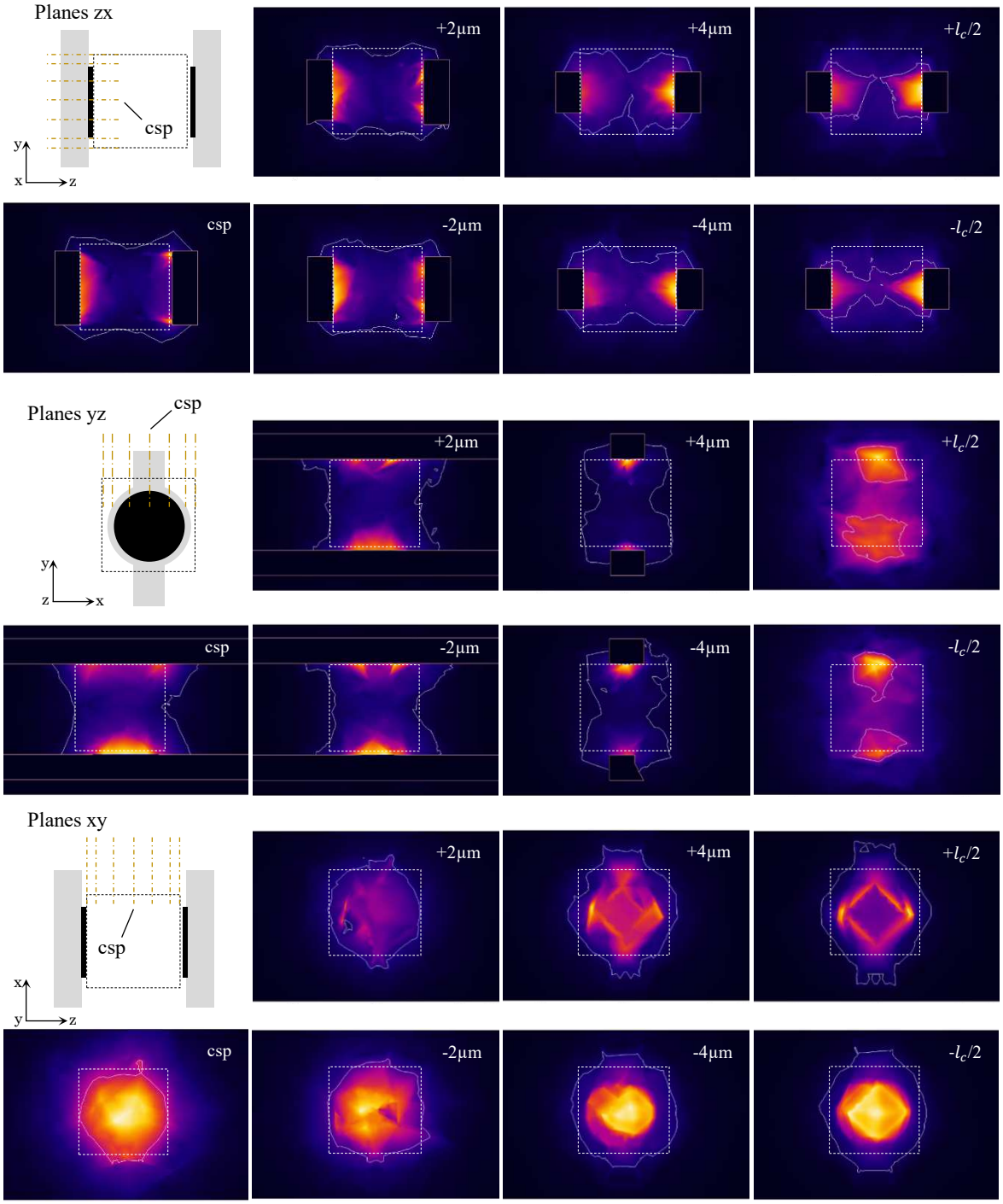

Figure 3. Volume enclosed by the threshold average boundary-peak stimulus for generating the stimulation cube. This volume was obtained from the surface/contour feature in COMSOL Multiphysics. The white line in the plots represents the zone for penetration depth for stimulation across the geometry. Dashed-line squares represent accurately the dimensions of the stimulation cube. Groups of planes (zx, xy, yz) illustrate the electrical current distribution in conductive and capacitive media. Together, each group corresponds of seven sub-planes located at a distance of ($\pm l_c/2$, ±4e-6, ±2e-6) µm away from the center sub-plane (csp). l_c represents the cube length.

Advance carrier technology should not add substantial size to the electronics since the total implant dimensions require a small-sized device to safely fit in the eye and ideally fit inside the orbit. Epiretinal implant size is limited because of the small incisions that can be safely made in the eyewall [Weiland, 2014]. The total chip surface area can be assembled using attachments of layers to minimize the total area. As a result, the total width

of one layer is computed as wn_i, and the total length of one layer is computed as ln_j. Where n_i and n_j are the number of columns and rows of single ASICs. To accommodate the electronics that control 1024 electrodes, 16 ASICs of 64 electrodes each is required [Meza-Cuevas et al., 2014]. We selected a two-layer arrangement of 2x4 each to minimize the total area of their attachment. The width and length of one layer are 15.7 and 8.4mm, respectively. The total area of a single layer is 1.32cm^2. The height between the layers is can be fixed to 1 mm.

4.3 3D Electrode Carrier´s Key Features

Visual prostheses would ideally reproduce accurately natural spatiotemporal patterns of activity in RGCs. This requires the capacity of each electrode to reach single-cell selectively. In other words, RGCs are tightly-packed in the ganglionic layer, mainly at the fovea. Unique characteristics of the visual space are sent to the brain via temporal patterns of activity in RGC types that are spatially mixed. RGCs that are close to each other frequently transmit very different signals.

It's not a secret that despite the challenges to overcome functional vision, fundamental research stipulated around 1000+ electrodes per single array are needed to upgrade basic issues such as mobility, independent living and navigating on the interior and exterior environments. Currently, a small number of companies such as Second Sight Medical Products (SS), Retina Implant GmbH (RI) and Intelligent Medical Implants GmbH (IMI) have developed a complete visual prosthesis device. Electrode diameters of IMI, RI, and SS are 100 and 360, 70 and 200 µm, respectively. Retinal implant devices previously stated likely activate hundreds of ganglion cells simultaneously over a particular region due to the size of the electrode used. Beyond just this coarse stimulation of cells restricts spatial resolution, the activity generated by stimulation remains dissimilar from a healthy retina too. Thus, those vision progresses need a significant enhancement to restore functional vision.

[Mahadevappa, 2005] found that the threshold current to activate ganglion cells was found to increase with time of surgery. The main reason is most likely the lifting off of the array from the underlying tissue. Simulation-based studies have been underscored the importance of controlling the distance between the array and the retina surface [Lujan et al. (a), 2016; Lujan et al. (b), 2016]. Therewith the problem lays the charge density to activate cells because charge density becomes proportional to the square of cell-electrode distance [Lujan et al. (b), 2016]. Despite that safe stimulus is delivered by approaching the electrode carrier to the surface of the retina, however, surgical challenges are thus delivered to maintain the proximity as close as possible. Close proximity of RGC to the electrodes reduces threshold stimulus allowing small electrodes to generate phosphenes within safe heat limits [Fried et al., 2006].

As described in this report, the novel advance technology of 3D electrode array provides key features that successfully address major concerns of current visual prosthetic devices: 1) increase number of electrodes up to +1000 for high-resolution vision, 2) electrode size reduction for one-to-one electrode-ganglion cell stimulation, 3) proximity of cell to electrode reduction for lowering threshold stimulus (safe stimulus below electrochemical limits) and targeting single cells during stimulation, 4) reinforce vertical-thickness depth accuracy stimulation.

4.4 Considerations for practical applications

The advance carrier technology of the 3D electrode array could potentially provide a strategy to improve cell selectivity on epi-retinal stimulation in visual implants. This reflects the fact that active electrodes inject low stimulus causing small volumes of stimulation corresponding to the volume enclosed by a single cell. Connected with the fact that current distribution could create electrochemical reactions, however, RGC stimulation using the 3D electrode carrier can supply stimuli below the limits of electrochemical reactions. As an advantage, the electrode carrier dimension is highly dependent on the volumetric cell density at the ganglionic layer, which in turn generates the stimulation cube as $v = \rho_v^{-1}$. For any three-dimensional topography of RGCs, the response of this formulation can be accurate by outputting the volume required for potentially stimulate single cells. The inputs of the simulation framework include veridical vertical spatial distribution of RGCs in a perspective three-dimensional view, ganglionic layer thickness, realistic volumetric cell density and RGC diameter at 1 mm away from the foveal center.

[Santos et al., 1997] demonstrated the feasibility to implant a retinal device by indicating that 25% to 30% of ganglion cells are preserved in the inner retinal region in patients suffering critical Retinitis pigmentosa (RP)

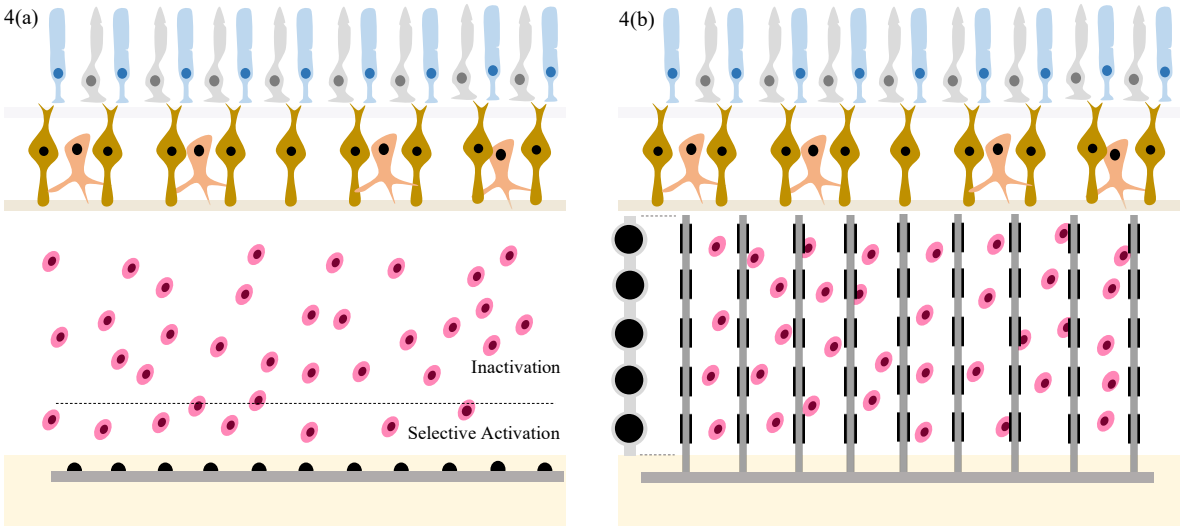

Figure 4. Selectivity activation comparison between 2D and 3D electrode carrier. Fig. 4(a) Flat 2D surface electrode arrays in visual implants distribute the current density radially in the retinal tissues expecting to stimulate selectivity a single RGC. Using this approach, accurate selective activation of RGC clearly provides complete negligence of cells placed deeply in the vertical segment of the ganglionic layer. Fig. 4(b) Precise stimulation of very-near and deep RGCs can be realized with the advance technology of the 3D electrode carrier. Any cell positioned randomly in the vertical segment of the ganglionic layer can accurately be activated by low threshold stimulus, preventing the generation of electrochemical reactions.

or Age-related macular degeneration (AMD). As a result, these experimental-based findings demonstrate that visually impaired patients suffering from RP or AMD can restore their sight using a visual prosthesis. Although courageously, though, a suitable visual prosthesis should be developed such that visual and detail perception yield natural spatiotemporal activity of cells. The applicability of the 3D carrier can accommodate the electrodes towards the generation of precise regions of stimulation.

5. Conclusion

In this report, the 3D electrode carrier is introduced. RGC localized stimulation is examined as the 3D carrier is placed at horizontal meridians (nasal and temporal) at the superior direction with the highest volume density of RGCs. This is required for a truthful restoration of natural RGC activity that likely requires independent activation of different cells. The simulation-based model obeyed the RGC density and distribution, ganglionic layer thickness, vertical distribution and the cell diameter at the location of 1 mm away from the fovea center. Our results indicate that electrode activation employing the 3D electrode carrier generates a volume of stimulation equivalent to the volume contained by a single RGC. Stimulation of small volume of the retina allows a more natural visual perception and replicates truthful spatiotemporal patterns of activity in the retina. The exposure of sensitive retinal tissue caused by electrochemical reactions is safeguarded as a result of the advanced technology of the 3D array that injects low thresholds for effective stimulation.

List of abbreviations

A_D – total chip surface area
I_a – applied current
P_{LSU} – power per LSU
P_t – power of the transistors that drive the electrodes
V_{DD} – voltage source
V_e – voltage drop across the electrodes
e_{ON} – the total number of transistors
e_d – depth of individual linear carrier
e_i – number of rows of linear carrier elements
e_j – number of columns of linear carrier elements
e_t – total number of electrodes
l_c – cube length
n_{ASIC} – number of ASICs
n_i – number of columns of single ASICs

n_j – number of rows of single ASICs
t_0 – initial time of stimulation
t_f – final time of stimulation
ρ_c – area cell density
ρ_v – volumetric cell density
ΔT – temperature change
Δt – pulse duration
A, B, C, D – numerical values of the 3rd order polynomial
I – peak threshold current
P – average power density of the device
Q – charge density
T – inverse of the total image frequency
csp – center sub-plane
f – total image frequency
l – total length of a single ASIC
r – electrode radius
v – volume contained by a single RGC
w – total width of a single ASIC
2D – two-dimension
3D – three-dimension
AMD – Age-related macular degeneration
IMI – Intelligent Medical Implants GmbH
LSU – Local Stimulation Unit
RGC – retinal ganglion cell
RI – Retina Implant GmbH
RP – Retinitis pigmentosa
SS – Second Sight Medical Products
VLARS – star-shaped very large electrode array for retinal stimulation

Ethics Approval and Consent to Participate
"Not applicable"

Consent for publication
"Not applicable"

Availability of supporting data
The datasets generated and/or analysed during the current study are available in the **Availability of data and materials** folder, repository: https://drive.google.com/drive/u/0/folders/1atupnGreI7SR0ciCCL54mIQoNjJ2nbFp

Competing interests
"The authors declare that they have no competing interests"

Funding
"Not applicable"

Authors' contributions
DLV carried out the conceptualization, methodology, use of software, interpretation of data, result validation, investigation, writing, software resources, and visualization. WHK carried out the conceptualization, second reviewer of result validation, writing - review & editing, supervision, and project administration. All authors read and approved the final manuscript

Acknowledgements
"Not applicable"

Authors' information
Dr.-Ing. Diego Lujan Villarreal, diego.lujan@tec.mx, Tecnológico de Monterrey, Escuela de Ingeniería y Ciencias. Av. Eugenio Garza Sada 2501 Sur, Tecnológico, 64849 Monterrey, Nuevo León, México.
Dr.-Ing. Wolfgang H. Krautschneider, krautschneider@tuhh.de. Hamburg University of Technology, TUHH, Hamburg, Germany

6. References

[1] Abramian M, Lovell NH, Morley JW, Suaning GJ, Dokos S. Computational Model of Electrical Stimulation of a Retinal Ganglion Cell with Hexagonally Arranged Electrodes. Conf Proc IEEE Eng Med Biol Soc. 2012;2012:3029-3032. PubMed PMID:23366563.

[2] Bagnoud M, SommerhalderJ, PelizzoneM, SafranAB. The amount of visual information required for the restoration of elementary reading abilities, using a retinal implant in patients with external retinal dystrophy: psychophysical study [in French]. Klin Monatsblat Augenheilk. 2001;218:360–362.
[3] Boretius, T., M. Schuettler, and T. Stieglitz. On the Stability of PEDOT as Coating Material for Active Neural Implants. 15th Annual Conference of the International Functional Electrical Stimulation Society, 2010
[4] Boycott, B. B. & Wässle, H. (1974). The morphological types of ganglion cells of the domestic cat's retina. Journal of Physiology 240, 397–419.
[5] Boycott, B., Dowling, J. (1969) Organization of the primate retina: light microscopy. Phil. Trans. 225, 109-184.
[6] Brindley GS, Lewin WS. The sensations produced by electrical stimulation of the visual cortex. J Physiol. 1968 May;196(2):479–493. PubMed Central PMCID: PMC1351724.
[7] Brummer S.B., M. J. Turner, "Electrochemical considerations for safe electrical stimulation of the nervous system with platinum electrodes," IEEE Tr Sohee ans. Biomed. Eng., vol. 24, no. 1, pp. 59–63, Jan. 1977.
[8] Cai, Q., et al. Response variability to high rates of electric stimulation in retinal ganglion cells. J Neurophysiology, 2011
[9] Cha K., Horch K W, R.A. Normann. Mobility performance with a pixelized vision system. Vision Research, 32 (1992), pp. 1367–1372
[10] Chader G., et al. Artificial vision: needs, functioning, and testing of retinal electronic prosthesis. Progress Brain Research, Vol. 175, 2009.Thompson R. W. Jr, G. David Barnett, Mark S. Humayun, Gislin Dagnelie. Facial Recognition Using Simulated Prosthetic Pixelized Vision. Investigative Ophthalmology & Visual Science, November 2003, Vol. 44, No. 11.
[11] Chai X., et al. Recognition of Pixelized Chinese Characters Using Simulated Prosthetic Vision. Artif Organs. 2007 Mar;31(3):175-82
[12] Chichilnisky, E.J. & Kalmar, Rachel. (2002). Functional Asymmetries in ON and OFF Ganglion Cells of Primate Retina. The Journal of neuroscience : the official journal of the Society for Neuroscience. 22. 2737-47. 10.1523/JNEUROSCI.22-07-02737.2002.
[13] Cook, J. E. (1997). Getting to grips with neuronal diversity: What is a neuronal type? In Development and Organization of the Retina: From Molecules to Function, pp. 91–120. Plenum Press, New York.
[14] Curcio C, Allen KA. Topography of Ganglion Cells in Human Retina. J Comp Neurol. 1990 Oct 1;300(1):5-25. PubMed PMID: 2229487.
[15] Da Cruz L., B. F. Coley, J. D. Dorn, F. Merlini, E. Filley, P. Christopher, F. K. Chen, F. Wuyyuru, J. A. Sahel, P. E. Stanga, M. S. Humayun, R. J. Greenberg, and G. Dagnelie, "The Argus II epiretinal prosthesis system allows letter and word reading and long-term function in patients with profound vision loss," Brit. J. Ophthalmol., vol. 97, no. 5, pp. 632– 636, May 2013].
[16] Dacey DM (2004) Origins of perception: retinal ganglion cell diversity and the creation of parallel visual pathways. In: The cognitive neurosciences (Gazzaniga MS, ed), pp 281–301. Cambridge, MA: MIT.
[17] Dacey, D. M. (1999). Primate retina: Cell types, circuits and color opponency. Progress in Retinal and Eye Research18, 737–763.
[18] Dagnelie G., David Barnett; Mark S. Humayun; Robert W. Thompson, Jr. Paragraph Text Reading Using a Pixelized Prosthetic Vision Simulator: Parameter Dependence and Task Learning in Free-Viewing Conditions. Investigative Ophthalmology & Visual Science March 2006, Vol.47, 1241-1250.
[19] Duay, J., Eleanor Gillette, Ran Liu, Sang Bok Lee. Highly flexible pseudocapacitor based on freestanding heterogeneous MnO2/conductive polymer nanowire arrays. Phys. Chem. Chem. Phys., 2012, 14, 3329–3337.
[20] Dumitru Petrusca, Matthew I. Grivich, Alexander Sher, Greg D. Field, Jeffrey L. Gauthier, Martin Greschner, Jonathon Shlens, E. J. Chichilnisky, Alan M. Litke. Identification and Characterization of a Y-Like Primate Retinal Ganglion Cell Type. Journal of Neuroscience 10 October 2007, 27 (41) 11019-11027; DOI: 10.1523/JNEUROSCI.2836-07.2007
[21] Eger M., Reinhard Eckhorn, Marcus Wilms, Thomas Schanze. Visual resolution with retinal implants estimated from recordings in cat visual cortex. Vision Research 46 (2006) 2675–2690
[22] Enroth-Cugell & Robson, J. G. (1966). The contrast sensitivity of retinal ganglion cells of the cat. Journal of Physiology187, 517–552.
[23] Fohlmeister J, PA Coleman, RF Miller. Modeling the repetitive firing of retinal ganglion cells. Brain Res. 1990 Mar 5;510(2):343-345. PubMed PMID: 2331606.
[24] Fried S, Hsueh HA, Werblin FS. A Method for Generating Precise Temporal Patterns of Retinal Spiking Using Prosthetic Stimulation. J Neurophysiol. 2006 Feb;95(2):970–978. PubMed PMID: 16236780.
[25] Greenberg RJ, TJ Velte, MS Humayun, GN Scarlatis, E de Juan. A computational model of electrical stimulation of the retinal ganglion cell. IEEE Trans Biomed Eng. 1999 May;46(5):505-514.
[26] Grumet AE (1999) Electric stimulation parameters for an epi-retina lprosthesis (dissertation). Cambridge MA, Massachusetts Institute of Technology.
[27] Hodgkin A, Huxley AF. A quantitative description of membrane current and its application to conduction and excitation in nerve. J Physiol. 1952 Aug 2;117(4):500-544. PubMed PMID: 1392413.
[28] Horsager A., & Fine, I. (2011). The perceptual effects of chronic retinal stimulation. In Visual Prosthetics: Physiology, Bioengineering, Rehabilitation. (pp. 271-300). Springer US. DOI: 10.1007/978-1-4419-0754-7_14.
[29] Hosseinzadeh Z, Jalligampala A, Zrenner E, Rathbun D, -L: The Spatial Extent of Epiretinal Electrical Stimulation in the Healthy Mouse Retina. Neurosignals 2017;25:15-25. doi: 10.1159/000479459
[30] Hottowy P, Skoczen´ A, Gunning DE, Kachiguine S, Mathieson K, Sher A, Wia˛cekP,LitkeAM,Da˛browskiW (2012) Properties and application of a multichannel integrated circuit for low-artifact, patterned electrical stimulation of neural tissue. J Neural Eng 9:066005. CrossRef Medline
[31] Humayun M. S., J. D. Dorn, L. Da Cruz, G Dagnelie, J. A. Sahel, P. E. Stanga, A. V. Cideciyan, J. L. Duncan, D. Eliott, E. Filley, A. C. Ho, A. Santos, A. B. Safran, A. Arditi, L. V. Del Priore, and R. J. Greenberg, "Interim results from the international trial of second sight's visual prosthesis," Ophthalmology, vol. 119, no. 4, pp. 779–788, Apr. 2012
[32] Humayun M. S., Olmos de Koo L. C. Retinal Prosthesis: A Clinical Guide to Successful Implementation. Springer, 2018
[33] Humayun MS, de Juan E Jr, Dagnelie G, Greenberg RJ, Probst RH, Phillips DH, et al. Visual perception elicited by electrical stimulation of retina in blind humans. Arch Ophthalmol. 1996 Jan;114(1):40– 46. PubMed PMID: 8540849.
[34] Humayun MS, Weiland JD, Fujii GY, Greenberg R, Williamson R, Little J, et al. Visual perception in a blind subject with a chronic microelectrode retinal prosthesis. Vision Res. 2003 Nov;43(24):2573– 2581. PubMed PMID: 13129543.
[35] Jensen RJ, Ofer R Ziv, Joseph F Rizzo. Thresholds for Activation of Rabbit Retinal Ganglion Cells with Relatively Large, Extracellular Microelectrodes. Invest Ophthalmol Vis Sci. 2005 Apr;46(4):1486–1496.
[36] Jepson LH, Hottowy P, Gunning DE, Litke AM, Mathieson K, et al. Focal Electrical Stimulation of Major Ganglion Cell Types in the Primate Retina for the Design of Visual Prostheses. J Neurosci. 2013 Apr 24;33(17):7194– 7205.

[37] Jepson LH, Hottowy P, Mathieson K, Gunning DE, Dąbrowski W, Litke AM, et al. Spatially Patterned Electrical Stimulation to Enhance Resolution of Retinal Prostheses. J Neurosci. 2014 April 2;34(14):4871– 4881. PubMed PMID: 24695706
[38] Joucla S, Glière A, Yvert B. Current approaches to model extracellular electrical neural micro stimulation. Front Comput Neurosci. 2014 Feb 19;8:13. PubMed PMID: 24600381.
[39] Kasi H., W. Hasenkamp, G. Cosendai, A Bertsch, and P. Renaud, "Simulation of epiretinal prostheses - Evaluation of geometrical factors affecting stimulation thresholds," Journal of Neuroengineering and Rehabilitation, vol. 8, no. 1, 2011.
[40] Kasi S, Brugger J, Renaud PH, de Rooij N, Cosendai G, Giungliano M. Analysis of Factors Affecting the Performance of Retinal Prostheses Using Finite Element Modelling of Electric Field Distribution in the Retina. PhD Thesis, June 2011.
[41] Klauke S. et al. Stimulation with a Wireless Intraocular Epiretinal Implant Elicits Visual Percepts in Blind Humans. Investigative Ophthalmology & Visual Science January 2011, Vol.52, 449-455. doi:10.1167/iovs.09-4410.
[42] Kolb H, Fernandez E, Nelson R, editors. Webvision: The Organization of the Retina and Visual System [Internet]. Salt Lake City (UT): University of Utah Health Sciences Center; 1995-. Available from: https://www.ncbi.nlm.nih.gov/books/NBK11530/
[43] Lohmann, Tibor & Haiss, et al. (2019). The very large electrode array for retinal stimulation (VLARS)-A concept study. Journal of Neural Engineering. 16. 10.1088/1741-2552/ab4113.
[44] Lujan Villarreal D (a), Schroeder D, Krautschneider WH. Biomimetic Stimulating Array for Single Localized Stimulation in Visual Prosthesis. Int J Comput Neural Eng. 2017;4(3):76 90. doi: http://dx.doi.org/10.19070/2572-7389-1700010
[45] Lujan Villarreal D (b), Schroeder D, Krautschneider WH. A Treatise of the Physical Aspects of Phosphenes and Single-Cell Selectivity in Retinal Stimulation. Int J Comput Neural Eng. 2017 Sep 23;4(2):55-70.
[46] Lujan Villarreal D. (a), Dietmar Schroeder, and Wolfgang H. Krautschneider, "Feasibility Study of a 1000+ Electrode Array in Epiretinal Prosthesis," International Journal of Pharma Medicine and Biological Sciences, Vol. 5, No. 3, pp. 163-170, July 2016. 10.18178/ ijpmbs.5.3.163170.
[47] Lujan Villarreal D. (b), Dietmar Schroeder and Wolfgang H. Krautschneider. Charge Density Study using Low Electrode Diameter in Epiretinal Prosthesis. ICTOpen2016 Conference. Amersfoort. The Netherlands. March 22 – 23, 2016.
[48] Lujan Villarreal D. Toward pixel-wise vision in epiretinal visual prosthesis. PhD thesis, Technische Universit¨at Hamburg-Harburg (2017). DOI: 10.15480/882.1454
[49] Lujan Villarreal D., Dietmar Schroeder and Wolfgang H. Krautschneider (2018) Retina Implant. European Patent No. WO/2019/057551. Retrieved from https://patentscope.wipo.int/search/en/detail.jsf?docId=WO2019057551.
[50] M. Meza-Cuevas, D. Schroeder, and W. H. Krautschneider, "A scalable 64 channel neurostimulator based on a hybrid architecture of current steering DAC," in Proc. Middle East Conference on Biomedical Engineering, 2014.
[51] M. Meza-Cuevas, D. Schroeder, and W. H. Krautschneider. (2012). Neuromuscular Electrical Stimulation Using Different Waveforms: Properties comparison by applying single pulses. 2012 5th International Conference on Biomedical Engineering and Informatics, BMEI 2012. 10.1109/BMEI.2012.6512988.
[52] Mahadevappa, M., Weiland, J., Yani, D., Fine, I., Greenberg, R., & Humayun, M. (2005). Perceptual thresholds and electrical impedance in 3 retinal prosthesis subjects. IEEE Transactions on Neural System Rehabilitation Engineering, 13, 201–206
[53] Merrill D. R., M. Bikson, and J. G. Jefferys, "Electrical stimulation of excitable tissue: Design of efficacious and safe protocols,"J. Neurosci. Methods , vol. 141, no. 2, pp. 171–198, Feb. 15, 2005.
[54] Nelson P, Aspinall P, Papasouliotis O, Worton B, O'Brien C. Quality of life in glaucoma and its relationship with visual function. J Glaucoma. 2003 Apr;12(12):139–150. PubMed PMID: 12671469
[55] Ong, J., et al. Effects of Cholesterol and Apolipoprotein E on Retinal Abnormalities in ApoE-Deficient Mice. Investigative Ophthalmology & Visual Science July 2001, Vol.42, 1891-1900.
[56] Piyathaisere D., E. Margalit; S. Chen; J. Shyu; S. D'Anna; J. Weiland; et. al. (2003). "Heat effects on the retina". Ophthalmic Surgery, Lasers, and Imaging 34 (2): 114–20
[57] Rattay F, Resatz S (2004) Effective electrode configuration for selective stimulation with inner eye prostheses. IEEE Trans Biomed Eng 51: 1659–1664. CrossRef Medline
[58] Ray A, Lee EJ, Humayun MS, Weiland JD (2011) Continuous electrical stimulation decreases retinal excitability but does not alter retinal morphology. J Neural Eng 8:045003. CrossRef Medline
[59] Raza A, Hood DC. Evaluation of the Structure–Function Relationship in Glaucoma Using a Novel Method for Estimating the Number of Retinal Ganglion Cells in the Human Retina. Invest Ophthalmol Vis Sci. 2015 Aug;56(9):5548-5556.
[60] Rizzo III J. F., Wyatt, J., Loewenstein, J., Kelly, S., & Shire, D. (2003). Perceptual efficacy of electrical stimulation of human retina with a microelectrode array during short-term surgical trials. Investigative Ophthalmology & Visual Science, 44, 5362–5369.
[61] Rizzo III JF, JL Wyatt, Loewenstein J, Kelly S, Shire D. Methods and Perceptual Thresholds for Short-Term Electrical Stimulation of Human Retina with Microelectrode Arrays. Investigative Ophthalmol Vis Sci. 2003 Dec;44(12):5355-61.
[62] Rodger DC, Fong AJ, Li W, Ameri H, Ahuja Ak, Zhong H, et al. Flexible parylene-based multielectrode array technology for high-density neural stimulation and recording. Sensors and Actuators B: Chemical. 2008 Jun 16;132(2):449-460.
[63] Rose TL, Robblee LS (1990) Electrical stimulation with Pt electrodes. VIII. Electrochemically safe charge injection limits with 0.2 ms pulses. IEEE Trans Biomed Eng 37:1118–1120. CrossRef Medline
[64] Ross MH, Kaye GI, Pawlina W: Histology, a Text and Atlas. 4th ed. Philadelphia: Lippincott Williams & Wilkins, 2003
[65] Rossi, Ethan & Granger, Charles & Sharma, Robin & Yang, Qiang & Saito, Kenichi & Schwarz, Christina & Walters, Sarah & Nozato, Koji & Zhang, Jie & Kawakami, Tomoaki & Fischer, William & Latchney, Lisa & Hunter, Jennifer & Chung, Mina & Williams, David. (2017). Imaging individual neurons in the retinal ganglion cell layer of the living eye. Proceedings of the National Academy of Sciences. 114. 201613445. 10.1073/pnas.1613445114.
[66] Rowe, M. H. & Stone, J. (1977). Naming of neurones. Classification and naming of cat retinal ganglion cells. Brain Behavior and Evolution14, 185–216.
[67] Ryskamp DA, Witkovsky P, Barabas P, Huang W, Koehler C, Akimov NP, et al. The Polymodal Ion Channel Transient Receptor Potential Vanilloid 4 Modulates Calcium Flux, Spiking Rate, and Apoptosis of Mouse Retinal Ganglion Cells. J Neurosci. 2011 May 11;3(19):7089 –7101. PubMed PMID: 21562271.
[68] Santos A, et al. Preservation of the Inner Retina in Retinitis Pigmentosa. A Morphometric Analysis. Arch Ophthalmol. 1997
[69] Seese T. M., H. Harasaki, G. M. Saidel, and C. R. Davies, "Characterization of tissue morphology, angiogenesis, and temperature in the adaptive response of muscle tissue in chronic heating," Lab. Investigation, vol. 78, pp. 1553–1562, 1998.

[70] Sekirnjak, Chris & Hottowy, Pawel & Sher, Alexander & Dabrowski, Wladyslaw & Litke, Alan & Chichilnisky, E.J.. (2008). High-Resolution Electrical Stimulation of Primate Retina for Epiretinal Implant Design. The Journal of neuroscience : the official journal of the Society for Neuroscience. 28. 4446-56. 10.1523/JNEUROSCI.5138-07.2008.
[71] Sohee Kim, et al. Preliminary study of the thermal impact of a microelectrode array implanted in the brain. Engineering in Medicine and Biology Society, 2006. EMBS'06. International Conference of the IEEE
[72] Starbird, R. et al. Electrochemical properties of PEDOT-NaPSS galvanostatically deposited from an aqueous micellar media for invasive electrodes, IEEE BMEICON, 2012.
[73] Stett A, Mai A, Herrmann T: Retinal charge sensitivity and spatial discrimination obtainable by subretinal implants: key lessons learned from isolated chicken retina. J Neural Eng 2007; 4:S7-16.
[74] Stingl K., K. U. Bartz Schmidt, D. Besch, A. Braun, A. Bruckmann, F. Gekeler, U. Greppmaier, S. Hipp, G. H¨ortd¨orfer, C. Kernstock, A. Kusnyerik, A. Schatz, K. T. Stingl, T. Peters, B. Wilhelm, and E. Zrenner, "Artificial vision with wirelessly powered subretinal electronic implant alpha-IMS," Proc. Royal Soc. B: Biol. Sci., vol. 280, no. 1757, pp. 1–8, Apr. 2013
[75] Veraart C, Raftopoulos C, Mortimer JT, Delbeke J, Pins D, Michaux G, et al. Visual sensations produced by optic nerve stimulation using an implanted self-sizing spiral cuff electrode. Brain Res. 1998 Nov;813(1):181–186. PubMed PMID: 9824694.
[76] Waschkowski, Florian & Hesse, et al. (2014). Development of very large electrode arrays for epiretinal stimulation (VLARS). Biomedical engineering online. 13. 11. 10.1186/1475-925X-13-11.
[77] Weiland J. D., and Mark S. Humayun. Retinal Prosthesis. IEEE Transactions on Biomedical Engineering, Vol. 61, No. 5, May 2014
[78] Werginz P, Benav H, Zrenner E, Rattay F. Modeling the response of ON and OFF retinal bipolar cells during electric stimulation. Vision Res. 2015 Jun;111(Pt B):170-81. PubMed PMID:25499837
[79] Wilke R, Gabel VP, Sachs H, Bartz Schmidt KU, Gekeler F, Besch D, et al. Spatial Resolution and Perception of Patterns Mediated by a Subretinal 16-Electrode Array in Patients Blinded by Hereditary Retinal Dystrophies. Invest Ophthalmol Visual Sci. 2011 Jul 29;52(8): 5995-6003. doi:10.1167/iovs.10-6946. PubMed PMID:21693599.
[80] Yin S, Lovell NH, Suaning GJ, Dokos S. A Continuum Model of the Retinal Network and its Response to Electrical Stimulation. Conf Proc IEEE Eng Med Biol Soc. 2010;2010:2077-80. PubMed PMID: 21095947.
[81] Zrenner E. (2002). "Will retinal implants restore vision?". Science 295: 1022–5.

Figures

1(a)

TABLE 2 DESCRIPTION OF THE VALUES OF SIMULATION

Layer	Conductivity [S/m]	Permittivity [-]	Thickness [µm]
Polyimide Carrier			10
LCE Length			60
LCE Depth	1e-17	1	2
LCE Outer Diameter[1]			9
LCE Width[2]			5
Vitreous Humor	1.5	98	50
Epithelium Layer	2e-3	1	65[1]
Photoreceptor Layer	28.5e-3	1	200
Intracellular space	10e-3	3.98e-11	30
PEDOT-NaPSS coating	400	1	0.2
Contact conductivity[3]	321	-	-
Cell membrane	1e-8	8.8e-11	0.01[4]
Inner nuclear layer	15e-3	1	100
Ganglionic Layer	10e-3	1	60

[1]Outer electrode diameter. [2]Width between electrodes. [3]Conductivity is of the contact of PEDOT-NaPSS deposition and tissue. [4]Cell membrane thickness.

1(b)

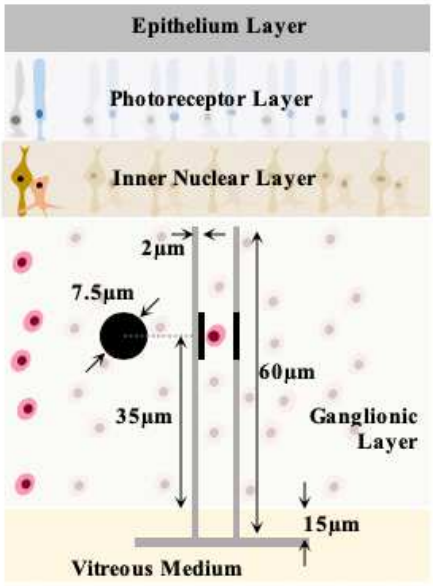

1(c)

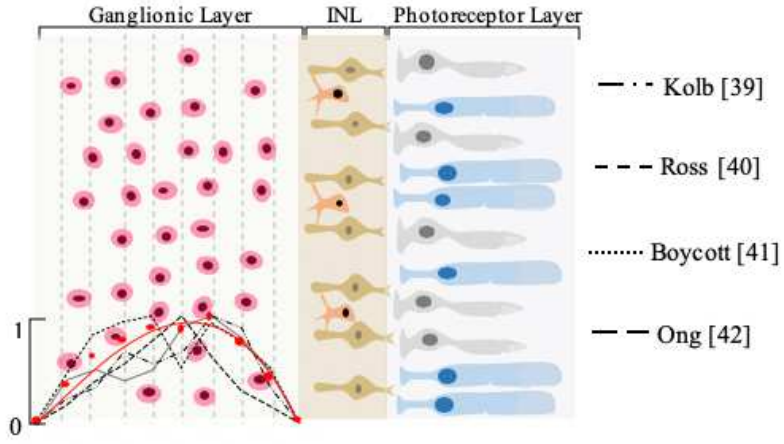

Figure 1

(a) 3D linear electrode carrier connected to an electrode connecting point can carry a plurality of the electrodes. Electrodes are arranged along a substantially straight line to penetrate into or through the surface of the ganglionic layer. Fig. 1(b) 3D retinal model implemented in Comsol Multiphysics (not drawn to scale). The model consists of tissue boxes that represent a segment of the human eye. A single pair of electrodes involving an active and ground is implemented using epi-retinal design. Fig. 1(c) Sketch of the retina along the vertical section. INL is the inner nuclear layer. Cell nuclei counting results are shown as a function of the ganglion layer thickness. The averaged and normalized results are plotted in

red with circular markers. The 3rd order polynomial is plotted in red with a solid line style. In addition, the normalized results of each reference are illustrated in black using four different line styles.

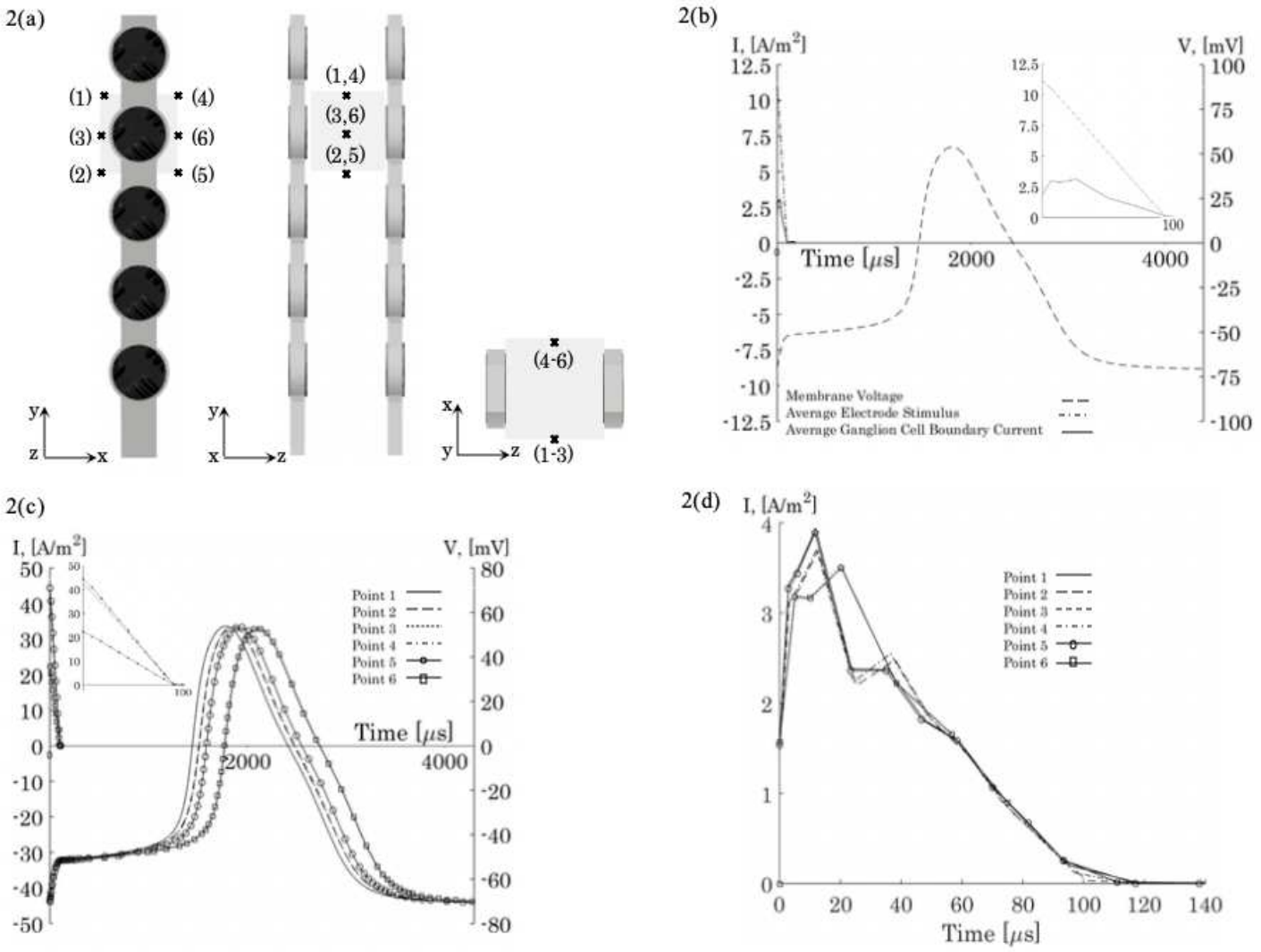

Figure 2

(a) Six different points of the cube to investigate the threshold current from the electrode. Note that all points are repeated based on the coordinate of interest. Fig. 2(b) threshold current density for exiting a single RGC. The cell is placed inside the ganglionic layer exactly between the linear carrier elements where the electrodes are located. Action potential is triggered with an average peak stimulus density of 11.31 A/m2 from the electrode. Single RGC located between active and ground electrodes obtains an average boundary-peak stimulus density of 3.1 A/m2 for stimulation. Fig. 2(c) threshold current density for generating the stimulation cube. Single RGC was placed in six different points to investigate membrane activation. Action potential is generated with an average peak stimulus density of 36.9 A/m2 from the electrode. Effective membrane stimulation required different values of electrode peak stimulus as the RGC shifted its position along the cube. Fig. 2(d) average boundary-peak stimulus density for effective stimulation of a single RGC located at six different points of the cube.

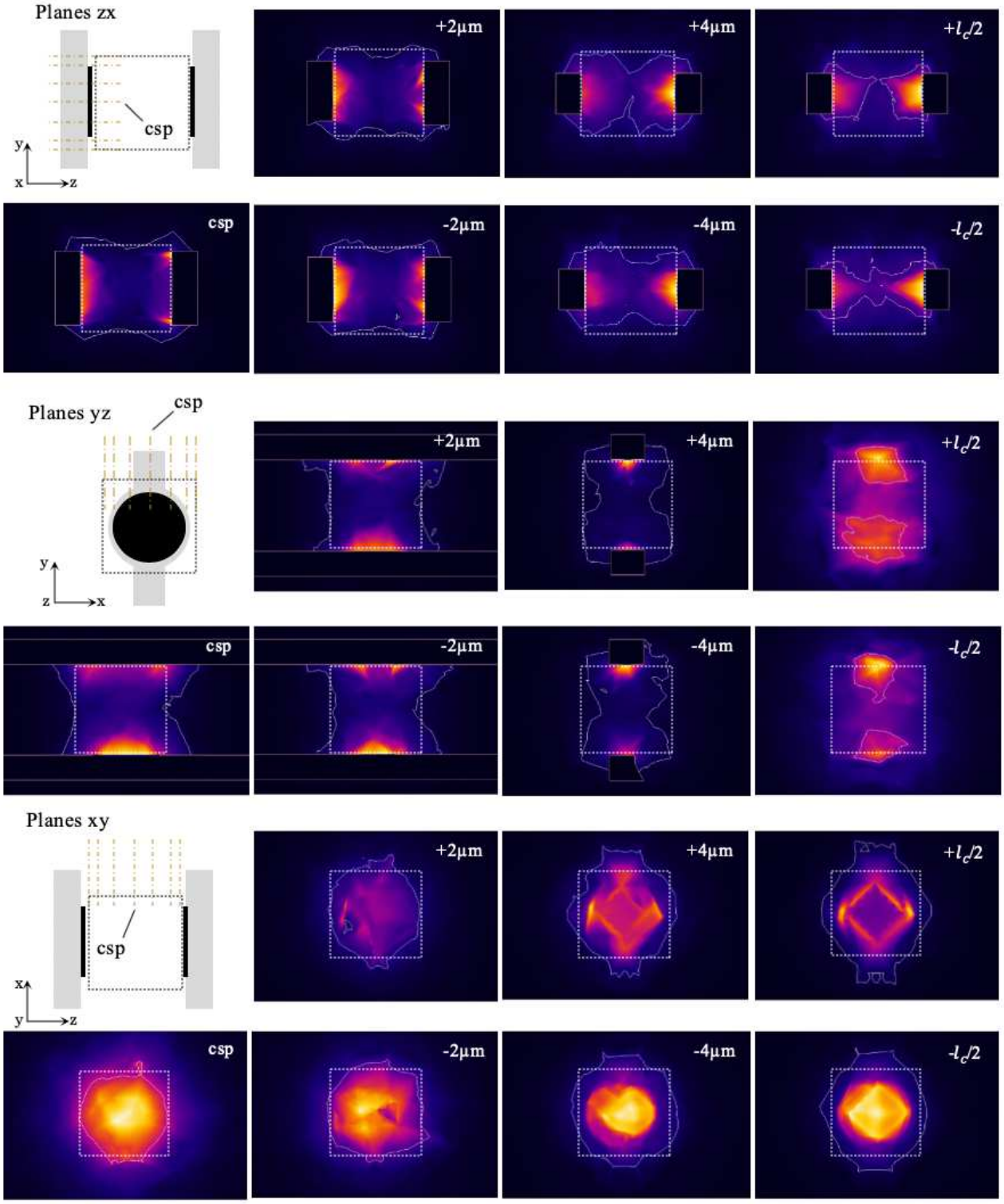

Figure 3

Volume enclosed by the threshold average boundary-peak stimulus for generating the stimulation cube. This volume was obtained from the surface/contour feature in COMSOL Multiphysics. The white line in the plots represents the zone for penetration depth for stimulation across the geometry. Dashed-line squares represent accurately the dimensions of the stimulation cube. Groups of planes (zx, xy, yz) illustrate the electrical current distribution in conductive and capacitive media. Together, each group

corresponds of seven sub-planes located at a distance of (±l_c/2, ±4e-6, ±2e-6) μm away from the center sub-plane (csp). l_c represents the cube length.

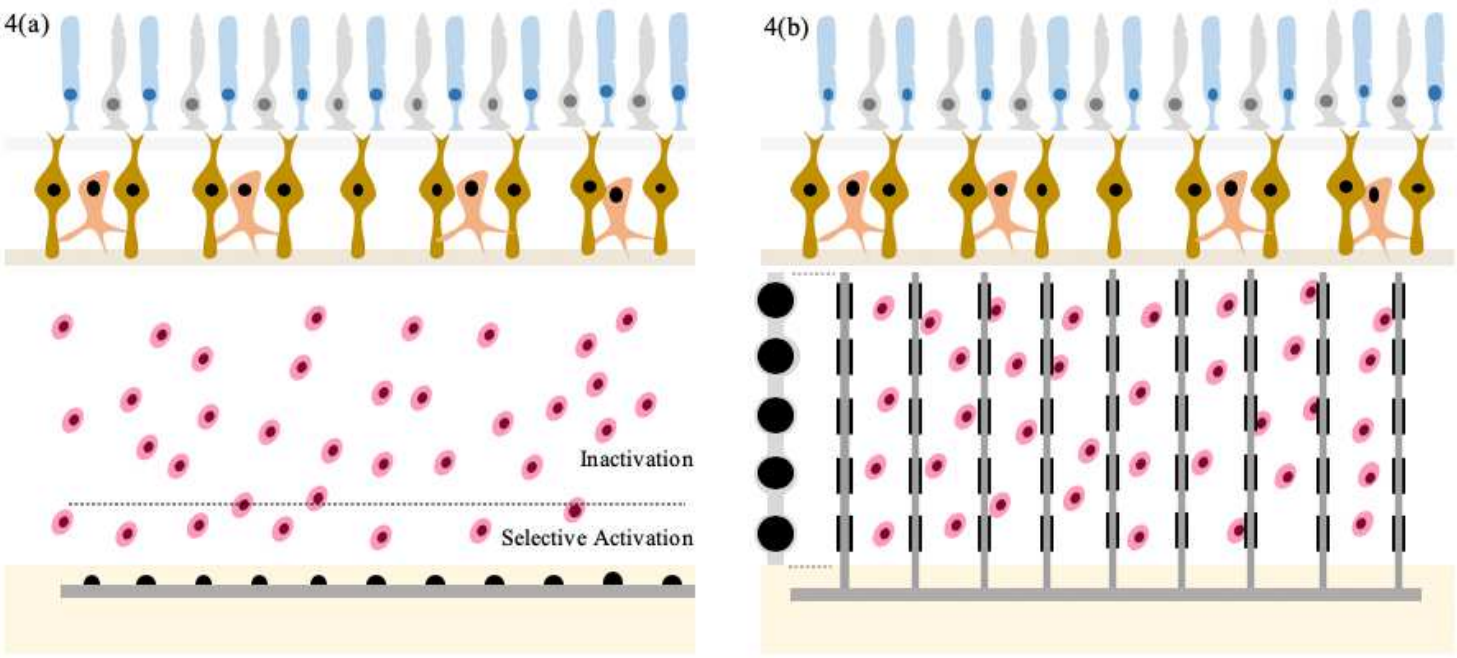

Figure 4

Selectivity activation comparison between 2D and 3D electrode carrier. Fig. 4(a) Flat 2D surface electrode arrays in visual implants distribute the current density radially in the retinal tissues expecting to stimulate selectivity a single RGC. Using this approach, accurate selective activation of RGC clearly provides complete negligence of cells placed deeply in the vertical segment of the ganglionic layer. Fig. 4(b) Precise stimulation of very-near and deep RGCs can be realized with the advance technology of the 3D electrode carrier. Any cell positioned randomly in the vertical segment of the ganglionic layer can accurately be activated by low threshold stimulus, preventing the generation of electrochemical reactions.